JOURNAL OF GENERAL VIROLOGY

RESEARCH ARTICLE

Vrijens *et al.*, *Journal of General Virology* 2019;100:583–601

DOI 10.1099/jgv.0.001235

MICROBIOLOGY SOCIETY

OPEN MICROBIOLOGY

Influenza virus entry via the GM3 ganglioside-mediated platelet-derived growth factor receptor β signalling pathway

Pieter Vrijens,[1] Sam Noppen,[1] Talitha Boogaerts,[1] Els Vanstreels,[1] Roberto Ronca,[2] Paola Chiodelli,[2] Manon Laporte,[1] Evelien Vanderlinden,[1] Sandra Liekens,[1] Annelies Stevaert[1] and Lieve Naesens[1,*]

Abstract

The possible resistance of influenza virus against existing antiviral drugs calls for new therapeutic concepts. One appealing strategy is to inhibit virus entry, in particular at the stage of internalization. This requires a better understanding of virus–host interactions during the entry process, including the role of receptor tyrosine kinases (RTKs). To search for cellular targets, we evaluated a panel of 276 protein kinase inhibitors in a multicycle antiviral assay in Madin-Darby canine kidney cells. The RTK inhibitor Ki8751 displayed robust anti-influenza A and B virus activity and was selected for mechanistic investigations. Ki8751 efficiently disrupted the endocytic process of influenza virus in different cell lines carrying platelet-derived growth factor receptor β (PDGFRβ), an RTK that is known to act at GM3 ganglioside-positive lipid rafts. The more efficient virus entry in CHO-K1 cells compared to the wild-type ancestor (CHO-wt) cells indicated a positive effect of GM3, which is abundant in CHO-K1 but not in CHO-wt cells. Entering virus localized to GM3-positive lipid rafts and the PDGFRβ-containing endosomal compartment. PDGFRβ/GM3-dependent virus internalization involved PDGFRβ phosphorylation, which was potently inhibited by Ki8751, and desialylation of activated PDGFRβ by the viral neuraminidase. Virus uptake coincided with strong activation of the Raf/MEK/Erk cascade, but not of PI3K/Akt or phospholipase C-γ. We conclude that influenza virus efficiently hijacks the GM3-enhanced PDGFRβ signalling pathway for cell penetration, providing an opportunity for host cell-targeting antiviral intervention.

INTRODUCTION

Human influenza A and B viruses are responsible for seasonal influenza with an estimated 5 million severe cases and 650 000 deaths worldwide [1]. In addition, zoonotic influenza A viruses can enter the human population to cause serious pandemics. Annual vaccination is limited by suboptimal vaccination rates, vaccine mismatches and only partial (60 % or less) effectiveness [2]. Hence, antiviral drugs are crucial to treat severe influenza virus infections in fragile individuals. At present, the only effective and globally available drugs are the neuraminidase (NA) inhibitors oseltamivir and zanamivir [3]. The worldwide oseltamivir resistance of H1N1 virus observed during 2007–2009 [4] underlines the need for entirely new antiviral strategies, some of which are in the clinical pipeline [5].

One innovative concept that aligns with a World Health Organization (WHO) call [6] is to target an influenza virus-associated host factor which is less prone to resistance. A plethora of host targets emerged from large RNA interference-based screenings and virus–host interactome analyses [7]. Targeting virus entry seems particularly attractive [8] as it shuts off all subsequent replication and pathogenic processes. A recent mouse study validated this approach with a drug blocking virus uptake via a Ca^{2+} channel receptor recently linked to influenza virus [9]. Influenza virus enters its host cells upon binding of the viral haemagglutinin (HA) to sialylated cell surface glycans [8, 10, 11]. After endocytosis followed by endosomal acidification, the virus undergoes M2-mediated uncoating coupled to HA-mediated fusion of the viral and endosomal membranes. In the last step of virus entry, the viral genome segments are transported from the

Received 1 October 2018; Accepted 1 February 2019; Published 14 February 2019

Author affiliations: [1]Department of Microbiology and Immunology, Rega Institute, KU Leuven, Leuven, Belgium; [2]Experimental Oncology and Immunology, Department of Molecular and Translational Medicine, University of Brescia, Brescia, Italy.

***Correspondence:** Lieve Naesens, lieve.naesens@kuleuven.be

Keywords: influenza virus; receptor tyrosine kinase; platelet-derived growth factor receptor; ganglioside; antiviral; virus entry.

Abbreviations: $CCID_{50}$, 50% cell culture infective dose; CHO, Chinese hamster ovary; CPE, cytopathic effect; DMEM, Dulbecco's modified Eagle medium; EGFR, epidermal growth factor receptor; EIPA, 5-(N-ethyl-N-isopropyl)amiloride; ERK, extracellular signal-regulated kinase; FGFR, fibroblast growth factor receptor; GalNAcT, β-1,4-*N*-acetylgalactosaminyltransferase 1; GEM, glycolipid-enriched membrane domain; HA, haemagglutinin; MCC, minimal cytotoxic concentration; MDCK, Madin-Darby canine kidney; NA, neuraminidase; NP, nucleoprotein; PDGFR, platelet-derived growth factor receptor; p.i., post-infection; PLC, phospholipase C; RTK, receptor tyrosine kinase; VEGFR, vascular endothelial growth factor receptor; vRNP, viral ribonucleoprotein.

One supplementary table and five supplementary figures are available with the online version of this article.

cytoplasm into the nucleus to initiate transcription and replication. One known route for influenza virion internalization is clathrin-mediated endocytosis [12, 13]. For another route depending on dynamin-2 GTPase, caveolae-mediated endocytosis, results are less consistent [14, 15]. In the presence of unknown serum components, the virus can enter via dynamin-independent macropinocytosis [16]. This route was described as more sensitive to receptor tyrosine kinase (RTK) inhibitors [16]. The fibroblast growth factor receptor (i.e. FGFR2 and FGFR4) was the first RTK to be linked to influenza virus entry [17]. Also, entering virus was shown to colocalize with the epidermal growth factor receptor (EGFR) and induce its activation and endocytosis [18]. RTKs share a similar structure consisting of an extracellular, transmembrane and cytoplasmic tyrosine kinase domain. Upon ligand binding to the extracellular domain, the receptors undergo dimerization and autophosphorylation, initiating signalling pathways to regulate cell growth, survival and proliferation. Cell surface expression of RTKs is controlled by endocytosis, which leads to receptor degradation or recycling [19]. Two prominent RTKs in inflammatory diseases of the airways [20] are EGFR and the platelet-derived growth factor receptor, which exists in two isoforms, PDGFR-α and PDGFR-β. Some RTK inhibitors are under investigation for chronic asthma [21].

To assess the relevance of RTK inhibitors for influenza therapy, it needs to be resolved whether some specific RTKs can give more efficient internalization, or whether additional cell surface factors play a modulating role. RTK signalling is regulated by gangliosides [22, 23], sialic acid-containing glycolipids which are concentrated in the lipid raft membrane regions from where RTK signalling initiates. The positive or negative regulation differs for diverse RTKs [22] and is governed by the precise ganglioside structure [23]. The possible association of gangliosides with influenza virus entry has not been thoroughly investigated. In one report, virus replication was slightly reduced in ganglioside-deficient cells [24]. In experiments with membrane models [25] or manipulated erythrocytes [26], gangliosides are used for their HA-binding capacity [27]. However, their potential role in post-binding virus internalization has not been investigated.

At the start of this study, a library of protein kinase inhibitors (including a subset acting on RTKs) was submitted for anti-influenza virus evaluation, with the aim of identifying protein kinase targets suitable for antiviral intervention. The RTK inhibitor Ki8751 showed superior efficacy and was subjected to mechanistic investigations. By comparing CHO-wild type and CHO-K1 cells, virus entry was proven to depend on the cell surface levels of GM1 and GM3 gangliosides. Entry via the PDGFRβ/GM3 axis was shown to involve desialylation of activated PDGFRβ by the viral NA, and coincide with strong activation of the extracellular signal-regulated kinase (Erk1/2) downstream effector pathway. Our findings are the first to delineate influenza virus entry via interplay between the viral HA and NA, cell surface RTKs and gangliosides. Interfering with this process by means of PDGFRβ inhibitors may be a valid strategy for influenza virus therapy.

METHODS

Chemical compounds

The library of 276 protein kinase inhibitors was purchased from Selleck Chemicals (catalogue no. L1200). Ki8751 [*N*-(2,4-difluorophenyl)-*N*′-(4-[(6,7-dimethoxy-4-quinolyl)-oxy]−2-fluorophenyl)urea [28]] and tivozanib were further purchased from the same company. Reference and control compounds were from commercial sources. The sulfated sialyl lipid NMSO3 [29] was a kind gift from T. Bowlin (Microbiotix).

Cells and viruses

Madin-Darby canine kidney (MDCK) cells, a kind gift from M. Matrosovich (Marburg, Germany) [30], and human embryonic kidney HEK-293T cells (Thermo Fisher Scientific HCL4517) were subcultivated in Dulbecco's modified Eagle medium (DMEM) supplemented with 10 % untreated FCS, 1 mM sodium pyruvate, and 750 mg sodium bicarbonate l^{-1}. Human airway epithelial Calu-3 cells (ATCC HTB-55) were subcultivated in MEM supplemented with 100 µM non-essential amino acids, 2 mM glutamine and 10 mM HEPES.

The Chinese hamster ovary ancestral cell line (herein called CHO-wild type; CHO-wt) and its CHO-K1 subclone were originally donated by J. D. Esko (University of California, La Jolla, CA, USA) and subcultivated in Ham's F12 medium supplemented with 10 % FCS and 2 mM glutamine. Stable CHO-FGFR4 transfectants were obtained by transfection of CHO-wt cells with the pCEP4 expression vector harbouring the human FGFR4 cDNA, followed by hygromycin selection [31]. CHO-K1-VEGFR2$^+$ (vascular endothelial growth factor receptor-2) transfectants were developed by a similar transfection procedure for human VEGFR2, combined with magnetic bead-based selection to achieve high-level VEGFR2 expression at the cell surface. Mouse anti-VEGFR2 antibody (Abcam ab9530) was bound to sheep anti-mouse IgG-coated Dynabeads (from Thermo Fisher Scientific), then mixed with VEGFR2-transfected CHO-K1 cells. By using a magnetic tube holder, cells attached to the Dynabeads were collected. Further selection under G418 yielded the CHO-K1-VEGFR2$^+$ cells. To obtain CHO-K1-GalNAcT cells, a pCMV6-entry plasmid encoding human β-1,4-*N*-acetylgalactosaminyltransferase 1 (GalNAcT) was purchased from Origene, and transfected into CHO-K1 cells using FuGENE 6 (from Promega). The cells were grown over 14 days in the presence of G418 to select a population that stably expressed the GalNAcT enzyme. During subcultivation, the CHO-FGFR4 and CHO-K1-GalNAcT cells were kept under G418. The antibiotic was omitted during one passage when cells were used for experiments.

In virus infection experiments with MDCK cells, the medium consisted of UltraMDCK medium (Lonza) with

225 mg sodium bicarbonate l^{-1}, 2 mM L-glutamine, and *N*-tosyl-L-phenylalanine chloromethyl ketone (TPCK)-treated trypsin at 2 μg ml^{-1}. For the CHO cells, the virus infection medium contained Ham's F12 medium with 2 mM L-glutamine and 0.4 % FCS.

Stocks of A/PR/8/34 influenza virus (ATCC VR-95) were prepared by intra-allantoic inoculation in embryonated hen eggs. For studies requiring a high m.o.i., 150 ml of allantoic stock was submitted to ultracentrifugation (3 h at 126 000 ***g***), after which the virus pellet was reconstituted in PBS and stored at −80 °C. Virus stocks were titrated by plaque assay in MDCK cells covered with 0.4 % agarose.

The A/WSN/33 virus was generated by reverse genetics [32] with a panel of eight plasmids [33] (a kind gift from R. Webster, Memphis), and expanded in embryonated hen eggs. Information on the additional influenza A and B virus strains can be found in Vanderlinden *et al.* [34].

Multicycle assays with influenza virus

The antiviral cytopathic effect (CPE) reduction assay was as described 35 [35]. Briefly, MDCK cells were seeded at 7500 cells per well into 96-well plates. One day later, influenza virus was added at an m.o.i. of 0.001 together with the test compounds at serial dilutions. After 3 days of incubation at 35 °C, viral CPE and compound cytotoxicity were scored by microscopy. Next, the MTS cell viability reagent (CellTiter 96 AQ_{ueous} MTS Reagent from Promega) was added, and 4 h later, absorbance at 490 nm was recorded in a Tecan Spark 10M plate reader.

For compound Ki8751, the microscopic CPE scores (i.e. score 0, 1, 2, 3 or 4 corresponding to 0, 25, 50, 75 or 100 % of the cells being lysed by the virus) in compound-treated virus-infected cells were expressed relative to the mock-treated virus control set at 100 %. The EC_{50} (50 % antivirally effective concentration) was calculated by interpolation based on the semi-log dose response. Compound cytotoxicity was expressed as the MCC (minimal cytotoxic concentration), i.e. the minimal test concentration producing visible alterations such as rounding, shrinking or lysis of the cells. In the MTS method, the EC_{50} and CC_{50} (50 % cytotoxic concentration) values were calculated by interpolation using the semi-log dose response. The percentage protection against virus was defined as: $[(OD_{Cpd})virus - (OD_{Contr})virus)]/[(OD_{Contr})mock - (OD_{Contr})virus] \times 100$, where $(OD_{Cpd})virus$ is the OD for a given concentration of the compound in virus-infected cells, $(OD_{Contr})virus$ is the OD for the untreated virus control and $(OD_{Contr})mock$ is the OD for the untreated mock-infected control. The percentage cytotoxicity was defined as: $[1 - (OD_{Cpd})mock/[(OD_{Contr})mock] \times 100$, where $(OD_{Cpd})mock$ is the OD for a given concentration of the compound in mock-infected wells.

For the virus yield assay [36], MDCK cells were seeded into 96-well plates at 25 000 cells per well. One day later, the cells were pre-incubated with compound over 15 min, and infected with influenza virus (m.o.i.: 0.001). After 24 h at 35 °C, the supernatants were frozen at −80 °C. In parallel, a mock-infected plate was incubated with the compounds over 72 h to determine the MCC by microscopy and CC_{50} by MTS cell viability assay. The virus in the supernatants was quantified by two methods. vRNA copy number was determined by one-step quantitative reverse transcription PCR (RT-qPCR) with two M-gene targeting primers and a matching probe plus M-plasmid standard [37]. All RT-qPCR analyses were run in duplicate. To determine the infectious virus titre, the supernatants were serially diluted in 96-well plates with MDCK cells (four wells per dilution). Three days later, microscopy was used to calculate the 50 % cell culture infective dose ($CCID_{50}$) according to the method of Reed and Muench [38]. Antiviral activity was calculated by interpolation and expressed as the EC_{90} and EC_{99} values, i.e. the compound concentrations to reduce by a factor of 10 and 100, respectively, the vRNA copy number or infectious virus titre.

One-cycle replication and virus binding experiments

Twenty-four-well plates were prepared with 125 000 MDCK or 175 000 CHO cells per well. On the next day, virus (m.o.i.: 0.01) was added together with compound (when applicable), except that in the time-of-addition assay, compound was added at different time points [−0.5, 0, 0.5, 1, 3, 5 or 8 h post-infection (p.i.)]. At 10 h p.i., supernatants were removed and total cell RNA extracts were prepared with the RNeasy mini kit (Qiagen). The vRNA copy number was determined by two-step RT-qPCR [37] using the M-gene directed primers and probe mentioned above. The qPCR analyses were run in duplicate.

To monitor the effect on virus binding, cells seeded in a 24-well plate were first exposed to the compound for 1 h at 35 °C. Next, the cells were cooled on ice for 10 min, virus was added and the plate was further cooled for 60 min. After removal of excess virus and two gentle washes with ice-cold medium, the cells were collected for total RNA extraction and two-step RT-qPCR analysis of vRNA, as explained above.

Immunofluorescence assays using confocal microscopy or flow cytometry

To monitor virus entry at 1 h p.i., MDCK, CHO or Calu-3 cells were seeded into eight-chamber glass slides (75 000 cells per well). One day later, the cells were incubated at 35 °C for 15 min with test compound (when applicable). Next, the slides were precooled, virus (m.o.i.: 30) was added, and the cells were put on ice for 60 min. Unbound virus was removed, test compound was again added and the slides were incubated for 1 h at 35 °C. For viral nucleoprotein (NP) immunostaining [34], the consecutive steps were (all done at room temperature and with antibodies diluted in 10 % goat serum in PBS): (i) three washes with PBS and 15 min fixation with 4 % formaldehyde; (ii) two PBS washes and 10 min permeabilization with 0.01 % Triton X-100; (iii) 30 min blocking with 10 % goat serum and 1 h

incubation with primary anti-NP antibody (ab20343 from Abcam; dilution 1 : 1000); (iv) two PBS washes and 1 h incubation with secondary antibody (A21131 from Thermo Fisher Scientific; dilution 1 : 500); and (v) two PBS washes and 10 min staining of the nuclei with DAPI (from Thermo Fisher Scientific). Finally, the cells were kept in PBS and analysed on a Leica TCS SP5 confocal microscope with excitation at 405, 488 or 566 nm and emission at 410–480 nm (blue DAPI signal), 495–565 nm (green) or 570–630 nm (red), respectively. All images were captured employing an HCX PL APO 63× (NA 1.2) water immersion objective. For quantitative analysis of nuclear entry, the green fluorescence signal per cell nucleus was analysed with Cell Profiler software (version 2.1.1) [39], starting from three images which each contained ~120 cells.

The same procedure as above was used to monitor virus entry in CHO-wt and CHO-K1 cells exposed to 80 µM dynasore, 80 µM EIPA [5-(*N*-ethyl-*N*-isopropyl)amiloride], 15 µM nocodazole, 30 µM chlorpromazine or 30 µM rhosin. When using 10 mM methyl-β-cyclodextrin, the cells were only exposed to the compound for 1 h of pre-incubation at 35 °C; virus binding and subsequent incubation at 35 °C were done in the absence of compound.

To perform dual staining for virus and ganglioside (GM1 or GM3) or PDGFRβ, the CHO cells were incubated with A/PR/8/34 virus (m.o.i.: 30) for 1 h on ice (for GM1/GM3 staining) or 10 min at 35 °C (for PDGFRβ). Next, immunostaining was performed as above, except that the cells were not permeabilized. Primary staining was done with anti-NP (same antibody as above), cholera toxin subunit B coupled to FITC (C1655 from Sigma-Aldrich; dilution 1 : 100) for GM1, anti-GM3 (NBT-M101-EX from Cosmo Bio; dilution 1 : 100) or anti-PDGFRβ (Ab32570 from Abcam; dilution 1 : 50). Secondary antibodies were: AF568-labelled goat anti-mouse IgG (A11004; dilution 1 : 250), Dy488-labelled donkey anti-rabbit IgG (SA5-10038; dilution 1 : 250) (both from Thermo Fisher Scientific) and AF488-labelled rat anti-mouse IgM (Biolegend No. 406522; dilution 1 : 50).

The expression levels of RTKs and gangliosides were measured by flow cytometry using established antibodies (see websites of the providers for more references). Confluent

Table 1. Activity of selected protein kinase inhibitors in an RT-qPCR-based influenza virus yield assay in MDCK cells

ND, Not determined.

Compound code	Kinase inhibitor profile*	Antiviral activity† (µM)		Cytotoxicity‡ (µM)	
		EC_{90}	EC_{99}	CC_{50}	MCC
Ki8751	VEGFR2, c-kit, PDGFRα, FGFR2	11	42	>200	>200
Tivozanib	VEGFR1/2/3, PDGFRα/β, c-Kit, FGFR1, c-Met	8.5	25	>100	33
Crenolanib	PDGFRα/β, Flt3	3.5	>4	8.0	ND
PP121	PDGFR, mTOR, hck, VEGFR2, Src, Abl, DNA-PK	3.7	5.4	14	8.1
Semaxanib	VEGFR2, PDGFRβ	60	>100	>100	ND
Motesanib	VEGFR1/2/3, PDGFR, Kit, Ret	<2.6	>6.4	>2.6	6.4
Dovitinib	VEGFR1/2/3, PDGFR, c-Kit, CSF-1R, FGFR1, FGFR3	3.7	>4	6.3	ND
Sunitinib	VEGFR2, PDGFRβ, Flt3, c-Kit	1.0	6.7	13	ND
Glesatinib	c-Met, RON, VEGFR1/2/3, Tie2	13	>20	95	30
Gefitinib	EGFR	5.5	13	41	ND
Imatinib	PDGFR, c-Kit	9.7	14	49	ND
PD173074	FGFR	11	16	36	ND
AZD4547	FGFR1/2/3/4, VEGFR2	17	>20	37	ND
AG-1024	IGF-1R, IR	1.9	3.8	20	4.7
MKK-2206	Akt	3.4	5.0	10	8.1
Apitolisib	mTOR, PI3K	13	21	9.2	>50
Sapanisertib	mTOR	11	32	31	37
U0126	MEK1/2	40	>50	18	13
SCH900776	Chk1, Chk2, CDK2	21	28	26	67
Roscovitine	Cdc2, CDK2, CDK5	7.9	15	>50	29
TAK-901	Aurora A/B kinase	2.2	2.9	4.6	2.9
Ribavirin	Not applicable	3.8	8.6	>100	>100

*Information from Selleck Chemicals.

†Based on RT-qPCR quantification of the vRNA copy number in the supernatant at 24 h p.i. The EC_{90} and EC_{99} correspond to the compound concentrations producing 10- and 100-fold reduction in vRNA copy number, respectively.

‡Cytotoxicity was assessed in mock-infected cells and expressed as the CC_{50}, i.e. 50 % cytotoxic concentration in the MTS cell viability assay; or MCC, i.e. minimal cytotoxic concentration producing microscopically visible alterations in cell morphology.

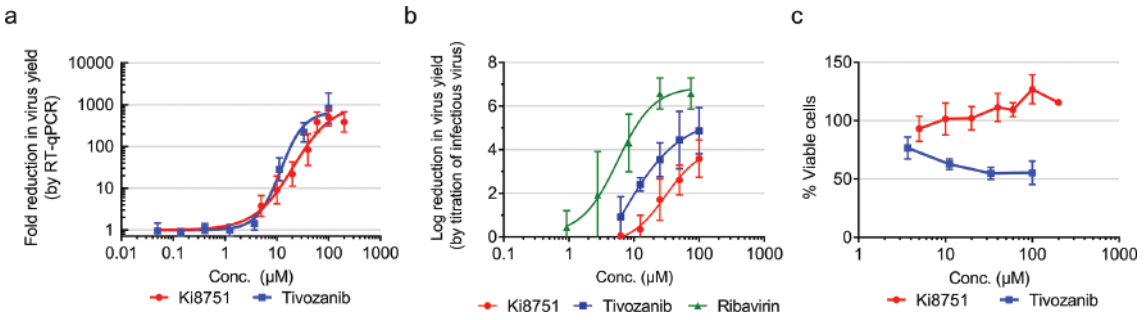

Fig. 1. Anti-influenza virus activity of Ki8751 and its structural analogue tivozanib. (a,b) Inhibitory effect in virus (A/PR/8/34)-infected MDCK cells, as monitored by virus yield assay on the supernatant at 24 h p.i., using (a) RT-qPCR quantification of vRNA genome copies and (b) titration of infectious virus. (c) Cytotoxicity in mock-infected MDCK cells, as assessed by MTS cell viability assay after 72 h of compound exposure. *N*=3 in each panel.

cell cultures were detached with non-enzymatic cell dissociation buffer (Sigma-Aldrich) and washed three times with FACS buffer (i.e. PBS plus 2 % FCS). About 400 000 cells were stained on ice, first with BD fixable viability stain 660 (BD Biosciences), then with primary antibody and, when applicable, the corresponding secondary antibody. All wash steps and antibody dilutions were carried out with FACS buffer. As control for non-specific background staining, a condition was included that was stained with secondary antibody only or an isotype control antibody (from BD Biosciences), i.e. IgG2a APC (No. 340473 at dilution 1 : 20) or IgG1a FITC/IgG2a PE (No. 342409 at dilution 1 : 5). For PDGFRβ staining, the cells were permeabilized with 100 % methanol for 30 min. The following monoclonal antibodies were used: anti-VEGFR2 (Abcam ab9530; dilution 1 : 50), PE-labelled anti-FGFR4 (BioLegend No. 324306; dilution 1 : 20), APC-labelled anti-FGFR2 (R and D systems FAB684A; dilution 1 : 20), anti-PDGFRβ (Santa Cruz sc-432; dilution 1 : 40), anti-EGFR (Santa Cruz sc-120; dilution 1 : 50) and anti-GM3 (Cosmo Bio NBT-M101-EX; dilution 1 : 50). For GM1-labelling, FITC-labelled cholera toxin B subunit (C1655 from Sigma-Aldrich) was used at a final concentration of 10 μg ml^{-1}. The secondary antibodies (all PE-labelled) were: goat anti-rabbit IgG (Thermo Fisher Scientific P2771MP; dilution 1 : 100), goat anti-mouse IgM (BioLegend No. 406508; dilution 1 : 40) and goat anti-mouse IgG (BioLegend No. 405307; dilution 1 : 50). Finally, the cells were analysed on a Becton-Dickinson FACSCanto II instrument, using FlowJo software for data analysis.

Experiment with influenza HA- and NA-pseudotyped lentivirus particles

The A/PR/8/34 HA and NA cDNA sequences were cloned into a pCAGEN plasmid [provided by C. Cepko via Addgene (No. 11 160)] [40]. Plasmid pCGGagPol was a gift from G. Maertens (Imperial College, London, UK) [41], while pQCXIP-AcGFP (derived from pQCXIP; Clontech) was donated by D. Daelemans (Rega Institute, Belgium). A published method [34] was used to produce GFP-expressing Moloney murine leukaemia virus particles carrying on their surface influenza virus H1 HA and N1 NA. HEK-293T cells were seeded in 60-mm dishes (2 500 000 cells per dish) using DMEM with 10 % FCS, then pre-incubated overnight. The cells were transfected with 10 μg pQCXIP-AcGFP, 8 μg pCGGagPol, 0.8 μg pCAGEN-HA and 0.2 μg pCAGEN-NA per dish, using a standard procedure with calcium phosphate (final concentration: 14 mM) diluted in HEPES-buffered saline [42]. One day later, the medium was replaced by Opti-MEM I (from Thermo Fisher Scientific), and on the next day, the supernatant was harvested. The HA0 protein on the pseudotyped particles was activated by 20 min of incubation with TPCK-treated trypsin at 10 μg ml^{-1}, followed by 20 min of incubation with soybean trypsin inhibitor at 5 μg ml^{-1}. Virus stocks were clarified by centrifugation (10 min at 1500 ***g***) and stored at −80 °C.

For lentiviral transduction, CHO cells were seeded into eight-well microscope slides (20 000 cells per well). On the following day, cells were transduced with pseudotyped particles and incubated for 72 h at 37 °C. Cell nuclei were then stained for 10 min with Hoechst 33 342 at 1 μg ml^{-1} (from Thermo Fisher Scientific) and transduction efficiency was estimated from the GFP signal monitored by High Content Imaging (CellInsight CX5, from Thermo Fisher Scientific). Quantitative image analysis was done with HCS studio software (version 6.6.0) on ~14 000 cells in total per condition.

Western blot analysis

CHO cells were seeded into 12-well plates at 375 000 cells per well, in Ham's F12 medium with 2 % FCS. On the next day, the cells were first starved in Ham's F12 medium without serum for 1 h and then pre-incubated with Ki8751 for 15 min at 35 °C. [In the experiment with zanamivir, details are provided in the relevant results section.] Next, the cells were incubated for the indicated time period with Ham's F12 medium containing human PDGF-BB at 50 ng ml^{-1} (homodimeric ligand for all PDGFR receptor types; from PeproTech), 20 % FCS or influenza virus (m.o.i.: 1000). After two washes with ice-cold PBS, protein extracts were made with ice-cold RIPA buffer supplemented with Halt

Table 2. Broad activity of Ki8751 against a broad set of influenza A and B virus strains

Data are the mean±SEM (*N*=3).

	Ki8751 (μM)		Ribavirin (μM)	
	EC_{50}* (CPE)	EC_{50}* (MTS)	EC_{50}* (CPE)	EC_{50}* (MTS)
A/H1N1				
A/PR/8/34	36±7	36±18	7.2±0.2	11±3
A/Ned/378/05	34±0	25±4	8.8±1.4	9.5±0.8
A/FM/1/47	63±15	85±13	13±1.7	17±6
A/Virginia/ATCC3/2009	34±0	38±1	9.3±2.0	9.5±2.0
A/WSN/33	41±3	47±6	6.4±0.8	9.4±1.8
A/H3N2				
A/HK/7/87	24±9	20±11	11±3	12±2
A/Ishikawa/7/82	35±11	35±11	8.3±1.0	6.8±1.6
A/X-31	18±8	28±14	12±2	7.4±3.3
A/Victoria/3/75	31±11	28±8	7.9±0.8	12±3
B				
B/HK/5/72	68±14	45±23	9.7±1.6	12±3
B/Ned/537/05	45±0	53±9	7.2±0.7	9.1±0.9
B/Lee/40	22±5	36±26	4.5±1.1	1.7±0.9
Toxicity† (CC_{50})	>100		>100	

*EC_{50} value: compound concentration producing 50 % inhibition of virus-induced cytopathicity in MDCK cells at day 3 p.i., as assessed by microscopic evaluation of the cytopathic effect (CPE) or by MTS cell viability assay.

†CC_{50} value: compound concentration producing 50 % cytotoxicity based on the MTS cell viability assay after 3 days of incubation with compound.

protease and phosphatase inhibitor mix (both from Thermo Fisher Scientific). Following Bradford analysis of total protein concentration, samples containing equal protein amounts were boiled after 4 : 1 mixing with reducing 5× Laemmli buffer. After protein separation on 3–8 % Criterion XT gels (Bio-Rad) and semi-dry blotting, the PVDF membranes were treated at 4 °C using 5 % BSA in PBST (PBS with 0.1 % Tween 20) as the blocking agent and 2 % BSA in PBST for all wash steps. The panel of primary antibodies contained: anti-phospho-PDGFRβ Tyr751 [No. 3161 from Cell Signaling Technology (CST); dilution 1 : 1000), anti-phospho-Erk1/2 Thr202/Tyr204 (No. 4370 from CST; dilution 1 : 2000), anti-phospho-Akt Ser473 (No. 4060 from CST; dilution 1 : 2000) and anti-phospho-PLC-γ1 Tyr783 (No. 2821 from CST; dilution 1 : 1000). The matching secondary antibodies were swine anti-rabbit HRP (P0399 from Dako; dilution 1 : 4000) and goat anti-mouse HRP (P0477 from Dako; dilution 1 : 10 000). Detection was done with SuperSignal West Pico chemiluminescence reagent (Thermo Fisher Scientific) and the ChemiDoc MP imaging system from Bio-Rad. After stripping (10 min exposure to Restore PLUS stripping buffer from Thermo Fisher Scientific), the membranes were detected for total PDGFRβ (Santa Cruz sc-432; dilution 1 : 200), Erk1/2 (CST No. 9102; dilution 1 : 1000), Akt (CST No. 4685; dilution 1 : 1000), PLC-γ1 (CST No. 2822; dilution 1 :1000) or β-actin (A5411 from Sigma-Aldrich; dilution 1 : 5000) followed by the same chemiluminescence detection procedure.

Statistical analysis

Differences between data sets were analysed with the unpaired two-sided Student's *t*-test without corrections [43]. $P \leq 0.05$ was set as the cut-off for statistical significance. Unless stated otherwise in the figure legends, the number of biological replicates (*N*) was 3.

RESULTS

Selection of Ki8751 from a broad protein kinase inhibitor library

The library of 276 inhibitors (listed in Table S1, available in the online version of this article) was first submitted to a CPE reduction assay in MDCK cells, using the A/WSN/33 influenza virus that was earlier applied in a genome-wide small interfering RNA study [17]. Most protein kinase inhibitors displayed pronounced cytotoxicity (see CC_{50} values determined by MTS assay; column F in Table S1). Twenty-nine compounds (marked in green in column D of Table S1) appeared to produce an inhibitory effect on the virus, as judged by microscopic inspection of the viral CPE. To determine their antiviral activity, these 29 molecules together with 20 prototype inhibitors of EGFR, PDGFR, VEGFR or FGFR were submitted to an RT-qPCR-based virus yield assay. In parallel, cytotoxicity was assessed by MTS and microscopic methods (Table 1: two right columns). Twenty-eight molecules proved to be inactive (marked in red in column E of Table S1). Among the 21 compounds producing 10- to 100-fold reduction in vRNA (see EC_{90} and EC_{99} values in Table 1), the RTK inhibitor

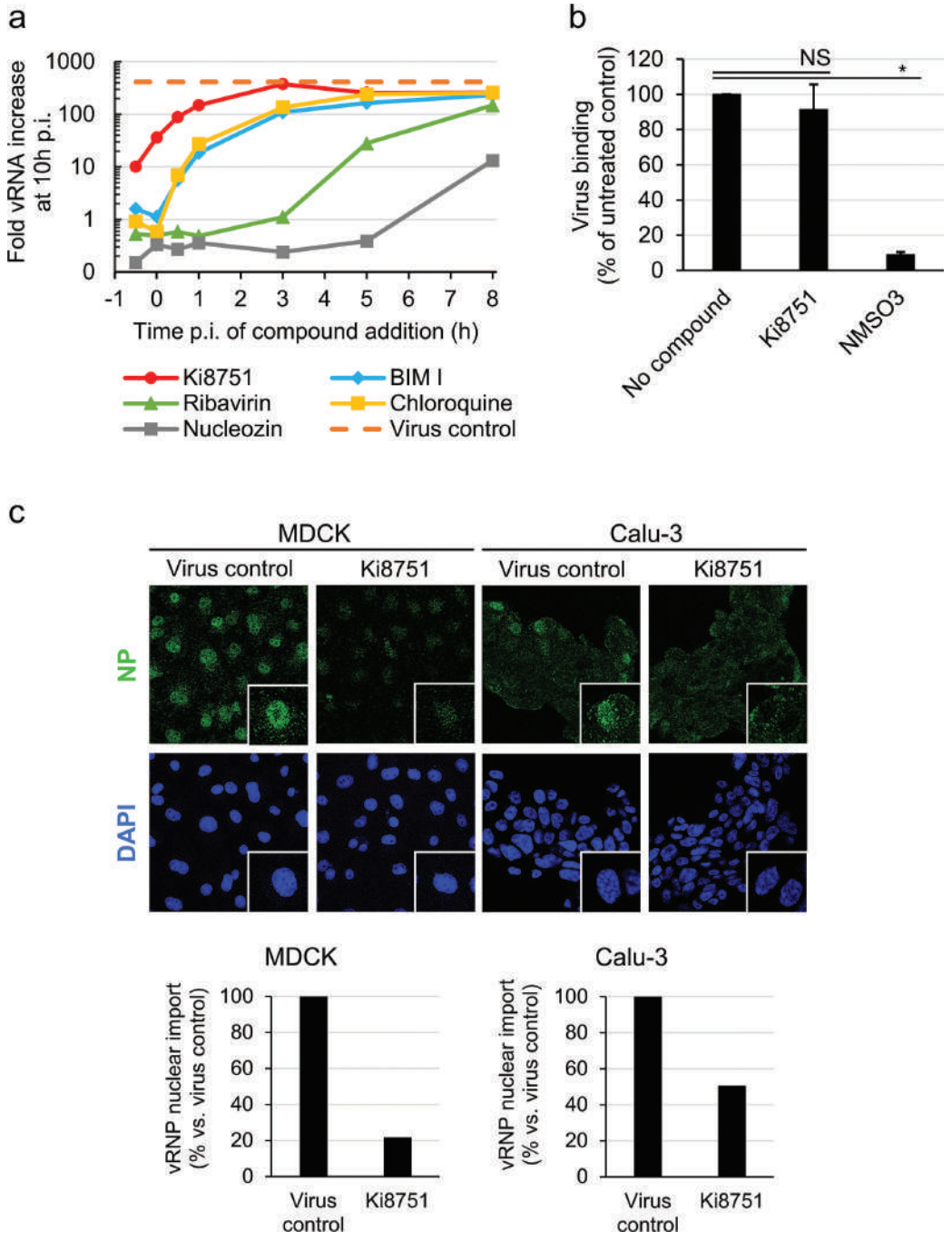

Fig. 2. Ki8751 acts prior to virus nuclear entry. (a) Time-of-addition experiment in influenza virus (A/PR/8/34)-infected MDCK cells. Compounds: 100 µM Ki8751, 20 µM bisindolylmaleimide I (BIM I), 25 µM ribavirin, 80 µM chloroquine and 1 µM nucleozin. The *y*-axis shows the fold increase in vRNA relative to the number of genome copies added at time zero. Dashed line: vRNA level in the virus control that received no compound. Mean values are shown (*N*=2). (b) Ki8751 has no effect on virus binding. After pre-incubating MDCK cells with compound for 60 min at 35 °C, followed by virus binding for 60 min at 4 °C, cell-bound virus was quantified by RT-qPCR. Compound concentrations: 20 µM for Ki8751 and 200 µM for the sulfated sialyl lipid compound NMSO3 [29]. The *y*-axis shows virus binding efficiency (mean±SEM; *N*=3) relative to untreated cells. **P*<0.05; NS=not significant (*P*>0.05). (c) Ki8751 (60 µM) inhibits virus nuclear entry in MDCK and Calu-3 cells. Confocal microscopy after NP-immunostaining at 1 h p.i. Green: viral NP; blue: nuclear DAPI staining. The bar diagrams show the quantified data from analysing ~120 cells per condition.

a

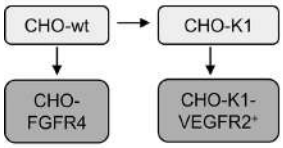

b

Cell line	% Cells staining positive for				
	FGFR4	VEGFR2	PDGFRα	PDGFRβ	EGFR
CHO-wt	0.31 ± 0.07	0.73 ± 0.26	1.2 ± 0.7	68 ± 18	0.64 ± 0.10
CHO-FGFR4	50 ± 11	1.3 ± 0.4	1.4 ± 0.6	62 ± 14	0.79 ± 0.25
CHO-K1	1.1 ± 0.9	0.62 ± 0.20	0.94 ± 0.48	79 ± 12	0.55 ± 0.15
CHO-K1-VEGFR2+	2.2 ± 0.2	40 ± 8	1.0 ± 0.3	49 ± 5	0.91 ± 0.25
MDCK	0.28 ± 0.07	0.99 ± 0.30	3.9 ± 2.3	43 ± 10	99 ± 1
Calu-3	0.41 ± 0.14	0.70 ± 0.04	2.0 ± 0.6	54 ± 6	99 ± 1

Fig. 3. RTK expression profile in the cell lines under study. (a) Relationship between the four CHO cell lines. CHO-K1 cells are a subclone of the CHO-wt ancestral cells (see: www.lgcstandards-atcc.org). CHO-FGFR4 cells are a stable FGFR4-transfectant derived from CHO-wt cells whereas CHO-K1-VEGFR2$^+$ cells are a stable VEGFR2-transfectant derived from CHO-K1 cells (see Methods). (b) Table summarizing the FACS results for the four CHO cell lines plus MDCK and Calu-3 cells. Mean±SEM (*N*=3). Representative FACS histograms are presented in Fig. S1.

Ki8751 stood out because of its superior selectivity with a CC_{50} to EC_{90} ratio of >18.

The other kinase inhibitors were not active and/or were less selective. A selectivity ratio of 10 was observed for AG-1024, an inhibitor of insulin-like growth factor 1 receptor and insulin receptor. Eleven EGFR inhibitors were evaluated yet only gefitinib [18] proved active. Some activity was seen for three inhibitors of the PI3K/Akt/mTOR pathway, i.e. MK-2206 [44], apitolisib and sapanisertib, besides two inhibitors of cyclin-dependent kinases [45], i.e. SCH900776 and roscovitine [46]. The MEK1/2 inhibitor U0126 [47] was active but poorly selective. Compound cytotoxicity probably explains why no antiviral effect was observed for the following molecules reported by others (see Table S1 for their cellular targets): PD153035 [18], SU11274 [18], staurosporine [16], wortmannin [16], tyrphostin AG879 [48], sirolimus [17], BI2536 [49], BEZ235 [50] and vemurafenib [51]. This discrepancy is plausibly linked to methodology. In our screen, a compound was regarded as active only when at least 10-fold reduction in virus yield was obtained at non- or subtoxic concentrations.

Ki8751 dose-dependently reduced the vRNA content in the supernatant, the reduction being 350-fold at 60 µM (Fig. 1a). Its strong (>3-$\log_{10}$ reduction) effect was confirmed by infectious virus yield assay (Fig. 1b). Ki8751 was devoid of cytotoxicity at 200 µM (Fig. 1c). It displayed broad anti-influenza A and B virus activity in the CPE assay, giving similar EC_{50} values by either microscopic or MTS assay (Table 2). Because the structural analogue tivozanib (recently approved in Europe for the treatment of advanced renal cell carcinoma) had similar antiviral activity yet higher cytotoxicity (Fig. 1), Ki8751 was chosen for further mechanistic studies. Besides its strong effect on VEGFR2, Ki8751 has >40-fold lower activity against PDGFRα, c-Kit and FGFR2 [28]. It is not active against EGFR.

Ki8751 acts prior to virus nuclear entry

In time-of-addition experiments, Ki8751 had the highest activity when added 0.5 h before virus infection; it was markedly less active when added at 0.5 or 1 h p.i. (Fig. 2a). Its time-of-addition curve preceded that of chloroquine, which acts at the endosomal stage of the virus by preventing endosomal acidification, and bisindolylmaleimide I, a protein kinase C inhibitor that blocks nuclear import of influenza viral ribonucleoprotein (vRNP) complexes [52]. Ki8751 was shown to have no effect on virus binding at 4 °C (Fig. 2b), whereas clear inhibition was seen with the sulfated sialyl lipid compound NMSO3 [29].

The early action point of Ki8751 was confirmed by confocal microscopy with quantitative analysis of vRNP imported in the nucleus at 1 h p.i. (Fig. 2c). Namely, Ki8751 (added 15 min before virus addition) impaired nuclear entry in MDCK (5-fold reduction of nuclear NP signal) and Calu-3 cells (2-fold reduction). The latter is a human airway epithelial cell line that resembles the natural human host cells [53].

Virus entry and activity of Ki8751 in CHO cell lines expressing PDGFRβ, FGFR4 or VEGFR2

We next moved to four CHO cell lines expressing some relevant RTK types (Fig. 3a). FGFR4 was previously linked to influenza virus entry [17] while VEGFR2 is particularly sensitive to Ki8751 [28]. The FGFR4-transfectant was derived from CHO-wt cells, whereas the VEGFR2-transfectant originated from CHO-K1 (Fig. 3a), and hence both parent cell lines were included. CHO-K1 is a subclone derived from CHO-wt ancestral cells (www.lgcstandards-atcc.org). The four CHO lines were highly positive for PDGFRβ yet negative for PDGFRα (Figs 3b and S1). They were also negative for EGFR (Fig. 3b) and FGFR2 (data not shown). The FACS data for expression of different RTKs in CHO and MDCK cells were confirmed by verifying mRNA expression using RT-qPCR (data not shown).

Quantitative confocal microscopy was performed to compare virus entry (as estimated from the NP signal at 1 h p.i.) in the four CHO cell lines. For FGFR4 and VEGFR2, the CHO transfectants showed the same entry efficiency as their respective parents (Fig. 4a). Strikingly, the NP signal at

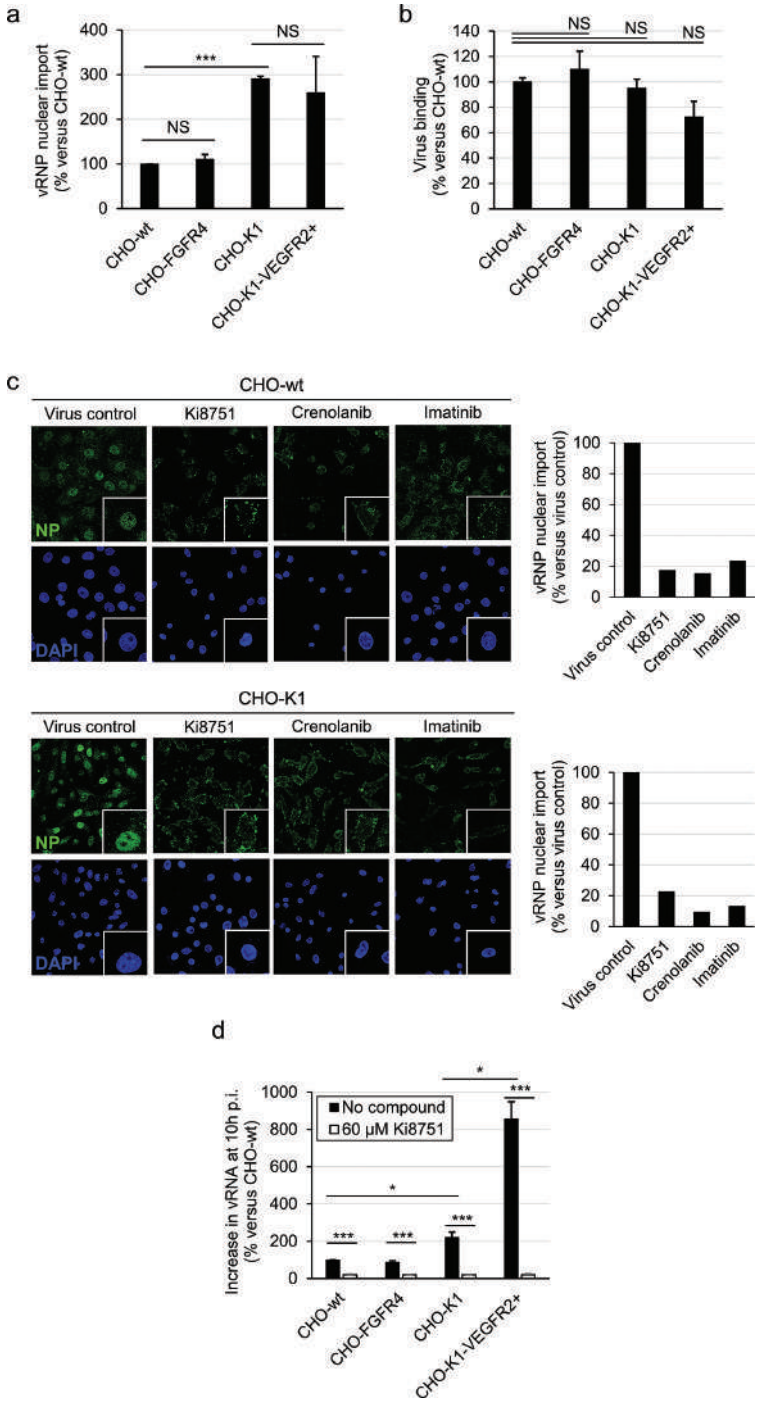

Fig. 4. Virus entry and inhibition by Ki8751 in CHO-wt, CHO-K1, and transfectant cells carrying FGFR4 or VEGFR2. (a) Nuclear import of vRNP in CHO cells incubated with influenza (A/PR/8/34) virus over 1 h at 35 °C. Quantitative confocal microscopy was carried out after dual nuclear staining for viral NP and DAPI. In three separate experiments, three images (each containing ~120 cells) were taken from each condition to quantify the green fluorescent signal in the nucleus. (b) Virus binding efficiency relative to CHO-wt cells, as determined by RT-qPCR quantification of cell-bound virus after 60 min of incubation at 4 °C. (c) Ki8751 and two other RTK inhibitors, crenolanib and imatinib (all at 60 µM), inhibit virus nuclear entry in CHO-wt and CHO-K1 cells. Confocal microscopy after NP-immunostaining at 1 h p.i. Green: viral NP; blue: nuclear DAPI staining. (d) vRNA synthesis at 10 h p.i., assessed by two-step RT-qPCR. The *y*-axis shows the fold increase in vRNA, relative to untreated CHO-wt cells. Panels a, b and d: mean±SEM (*N*=3). Statistical significance by two-sided Student's *t*-test: **P*<0.05; ****P*<0.005; NS=not significant (*P*>0.05).

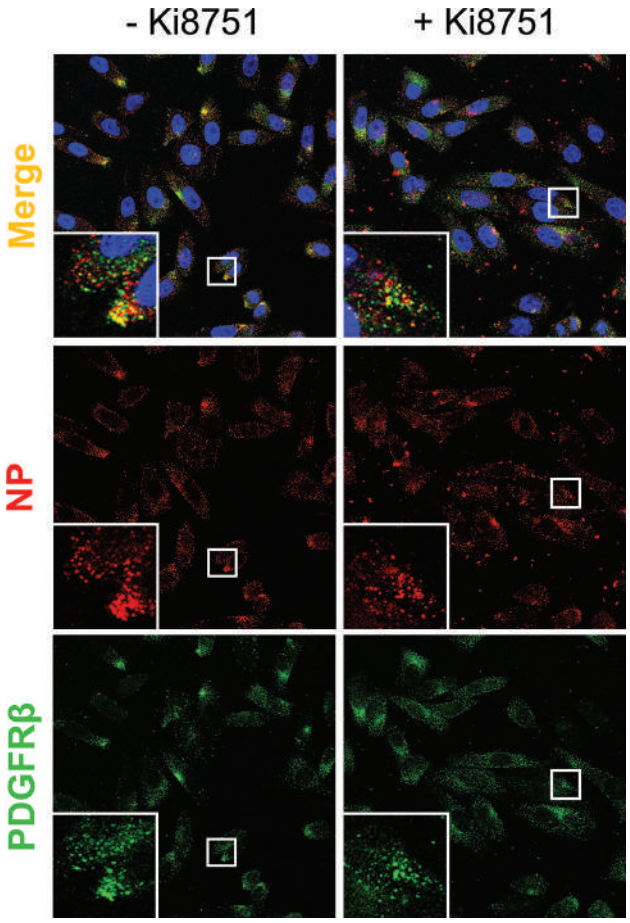

Fig. 5. Entering virus and PDGFRβ co-localize in the endosomal compartment. CHO-K1 cells were incubated with or without 60 µM Ki8751 for 15 min at 35 °C. Then, A/PR/8/34 virus was added and the cells were further incubated for 10 min at 35 °C. After fixation, cells were stained for NP (red) and PDGFRβ (green). In the upper panels, the yellow colour marks co-localization of virus and PDGFRβ. A close-up of the endosomal compartment of a specified cell is shown in the lower left corner of each picture.

1 h p.i. was more than three-fold and significantly (P<0.001) higher in CHO-K1 than in CHO-wt cells (Fig. 4a). This difference was not situated at the virus binding stage, as the four CHO cell lines behaved almost identically in a virus binding assay at 4 °C (Fig. 4b). Virus nuclear entry in CHO-K1 cells was as efficient as that seen in MDCK cells (Fig. S2).

In CHO-wt and CHO-K1 cells, virus import into the nucleus was strongly reduced in the presence of Ki8751 and two additional PDGFR inhibitors, crenolanib and imatinib (Fig. 4c). Overall, these three compounds reduced the nuclear NP signal by a factor of 5- to 10-fold. A similar degree of inhibition was seen with the endosomal V-ATPase inhibitor bafilomycin A1, while no effect was observed for the protein synthesis inhibitor cycloheximide, meaning that the nuclear NP signal at 1 h p.i. resulted from vRNP import into the nucleus (Fig. S3).

We also compared the level of viral vRNA synthesis at 10 h p.i. Compatible with their enhanced virus uptake, CHO-K1 cells produced two-fold higher (P<0.05) vRNA levels than CHO-wt cells (Fig. 4d). In all four CHO cell lines, influenza virus replication was fully inhibited by Ki8751 at 60 µM (Fig. 4d, white bars). Intriguingly, vRNA synthesis was considerably higher in CHO-K1-VEGFR2$^+$ cells compared to their CHO-K1 parent (P<0.05), although virus entry was similar in both (Fig. 4a). This suggests that VEGFR2 promotes vRNA synthesis at a stage beyond virus entry into the nucleus; the underlying mechanism is currently being explored.

Since Ki8751 was found to inhibit virus entry in MDCK, Calu-3 and the four CHO cell lines, and all these cells express PDGFRβ, we hypothesized a link between this RTK and virus entry. Dual immunostaining in CHO-K1 cells showed that PDGFRβ and entering virus were localized to the same endosomal compartment (Fig. 5). In the presence of Ki8751, this co-staining was less pronounced.

Opposite roles of GM1 and GM3 in influenza virus uptake

The above data showed that entry of influenza virus is three-fold more efficient in CHO-K1 compared to CHO-wt cells.

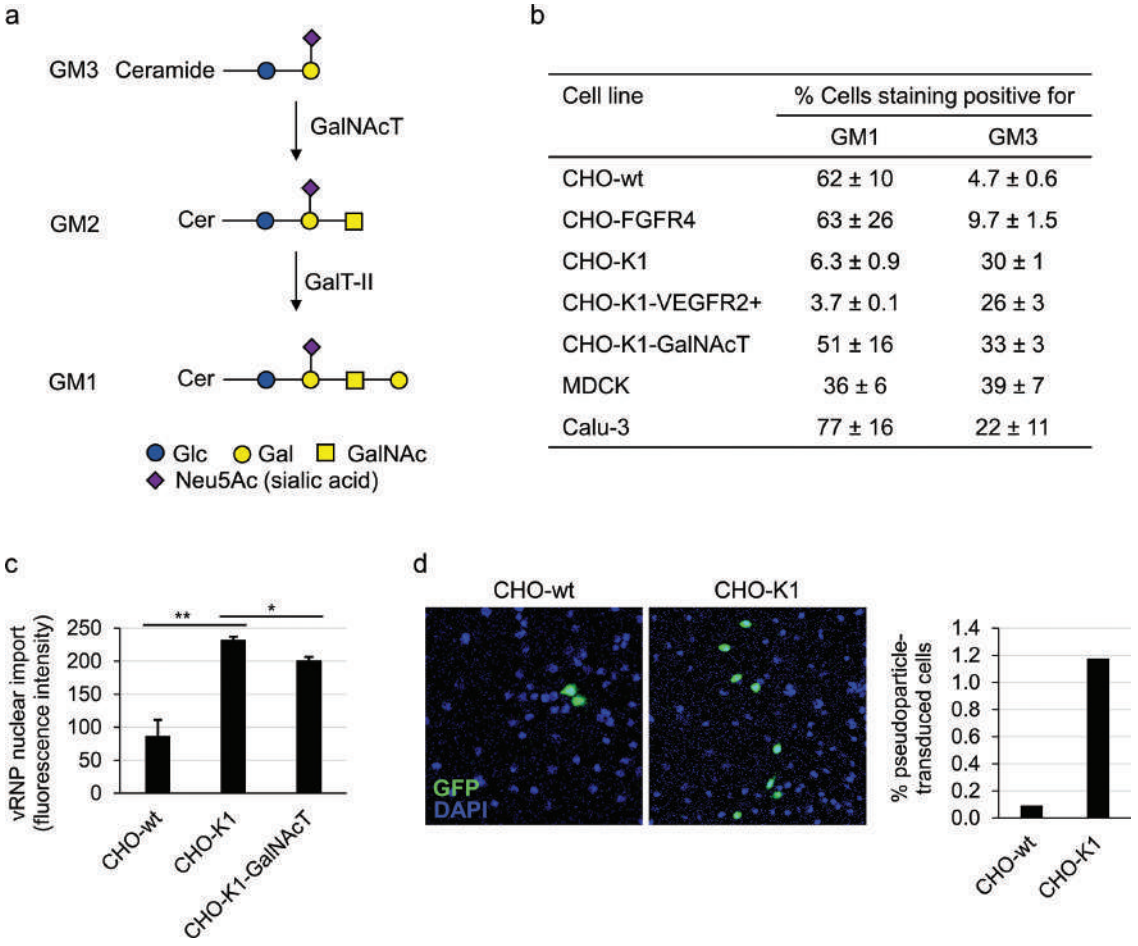

Cell line	% Cells staining positive for	
	GM1	GM3
CHO-wt	62 ± 10	4.7 ± 0.6
CHO-FGFR4	63 ± 26	9.7 ± 1.5
CHO-K1	6.3 ± 0.9	30 ± 1
CHO-K1-VEGFR2+	3.7 ± 0.1	26 ± 3
CHO-K1-GalNAcT	51 ± 16	33 ± 3
MDCK	36 ± 6	39 ± 7
Calu-3	77 ± 16	22 ± 11

Fig. 6. Impact of GM1/GM3 expression profile on influenza virus internalization. (a) Relevant steps in the ganglioside synthesis pathway. GalNAcT: β-1,4-*N*-acetylgalactosaminyltransferase 1; GalT-II: β-1–3-galactosyltransferase 2. (b) Surface expression of GM1 and GM3 gangliosides, based on FACS analysis. CHO-K1-GalNAcT: transfectant cells expressing the GalNAcT enzyme. Representative FACS histograms are shown in Fig. S4. (c) vRNP import at 1 h p.i. to assess the efficiency of virus uptake. **P*<0.05; ***P*<0.01 (two-sided Student's *t*-test). In (b) and (c), data are the mean±SEM (*N*=3). (d) Transduction of HA- and NA-bearing GFP-expressing pseudoparticles in CHO-wt and CHO-K1 cells. Nuclei were stained with Hoechst 33 342. Left: representative images; right: data obtained by quantitative image analysis on ~14 000 cells in total per condition to compensate for low transduction efficiency (mean of two independent experiments).

CHO-K1 cells lack the enzyme to convert GM3 to GM2 [54], which is further converted to GM1 (see Fig. 6a: the two reactions are catalysed by, respectively, GalNAcT and galactosyltransferase II (GalT-II)) [55]. FACS analysis (Figs 6b and S4) confirmed that CHO-K1 cells express more GM3 than GM1, while CHO-wt cells exhibit the opposite pattern. The CHO-K1-GalNAcT transfectant had a ratio of GM1-positive cells of 51 % compared to 6 % in its CHO-K1 parent (Fig. 6b). This increase in GM1 led to a reduction in virus entry (Fig. 6c). The reduction was significant (P<0.01) albeit quite modest, which can be explained by the fact that the ratio of GM3-positivity was relatively high (~30 %) in both the GalNAcT-transfectant and CHO-K1 parent. Nevertheless, the data agreed with our assumption that GM1 negatively affects influenza virus uptake while GM3 has a stimulating effect.

The difference between CHO-wt and CHO-K1 was even more pronounced when we used lentiviral pseudoparticles carrying influenza virus HA and NA, instead of intact virions. Although pseudoparticle transduction was quite inefficient, it was clearly (13-fold) higher in CHO-K1 compared to CHO-wt cells (Fig. 6d). This underlines that HA and NA are the primary (and probably exclusive) viral factors implicated in the ganglioside-modulated entry process.

The association between entering virus and GM3-positive lipid rafts was established by confocal microscopy with dual staining for viral NP and GM1 or GM3. In CHO-K1 and CHO-wt cells, the virus was prominently present in GM3-positive membrane regions (Fig. 7: two top right images). Some virus was detected in GM1-positive rafts of CHO-wt

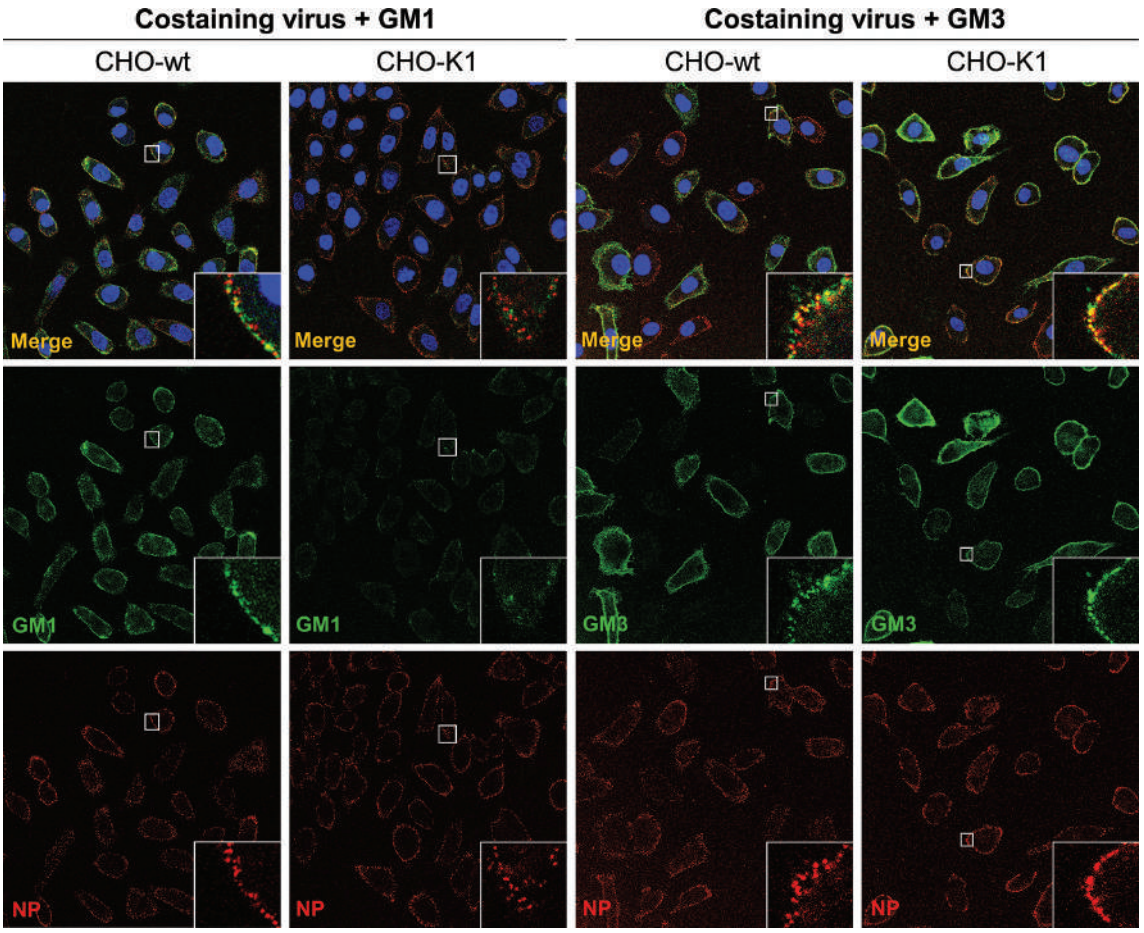

Fig. 7. Influenza virus prefers GM3-positive membrane regions. CHO-wt and CHO-K1 cells were incubated with A/PR/8/34 virus for 1 h on ice, then stained for NP (red), GM1 or GM3 (green) and the nucleus (DAPI in blue). In the upper panels, the yellow colour marks co-localization of virus and GM1 or GM3. A close-up of the membrane of a specified cell is shown in the lower right corner of each picture.

cells (top left image in Fig. 7), but this seemed less pronounced and restricted to a few spots on the cell surface.

Influenza virus entry increases PDGFRβ and Erk1/2 activation in CHO-K1 compared to CHO-wt cells

GM1 and GM3 are known to have opposite effects on PDGFRβ signalling [22, 23]. Hence, we compared the CHO-wt and CHO-K1 cells in terms of PDGFRβ activation and its inhibition by Ki8751. Upon stimulation with a high concentration (50 ng ml^{-1}) of the receptor ligand PDGF-BB, PDGFRβ phosphorylation was considerably higher in CHO-wt cells (having higher GM1-positivity) compared to CHO-K1 cells (having higher GM3-positivity) (Fig. 8a: compare lanes 3 and 9). As a result, PDGF-BB-treated CHO-wt cells showed higher activation of the Raf/MEK/Erk, PI3K/Akt and phospholipase C (PLC)-γ pathways (Fig. 8d). This was unexpected as it contradicted other reports that PDGFRβ activation is inhibited by GM1 but not by GM3 [23, 56, 57]. However, the last finding was confirmed with 20 % FCS as the stimulant, as the level of phosphorylated PDGFRβ was now three-fold higher in CHO-K1 than in CHO-wt cells (Fig. 8b: compare lanes 3 and 9); this difference was significant (P<0.01; Fig. 8e). The magnitude and kinetics of RTK signalling depend on ligand concentrations [58]; clearly, 20 % FCS is physiologically more relevant than 50 ng PDGF-BB ml^{-1}. In both cell lines, the FCS stimulus induced strong activation of the Akt and Erk pathways, giving prominent bands of pAkt and pErk1/2. The latter explained the small band shift in detection of total Erk1/2 [59]. The strong PDGFRβ signalling in CHO-K1 cells was also evident from their high level of basal receptor phosphorylation before any stimulus was added (see lane 7 in Fig. 8b). When exposed to influenza virus (Fig. 8c, f), their level of phosphorylated PDGFRβ was further, yet only slightly (P>0.1), increased. As a result, the phospho-PDGFRβ level at 10 min p.i. was markedly higher (18-fold, P<0.005) in CHO-K1 cells compared to that seen in CHO-wt cells (Fig. 8c, f).

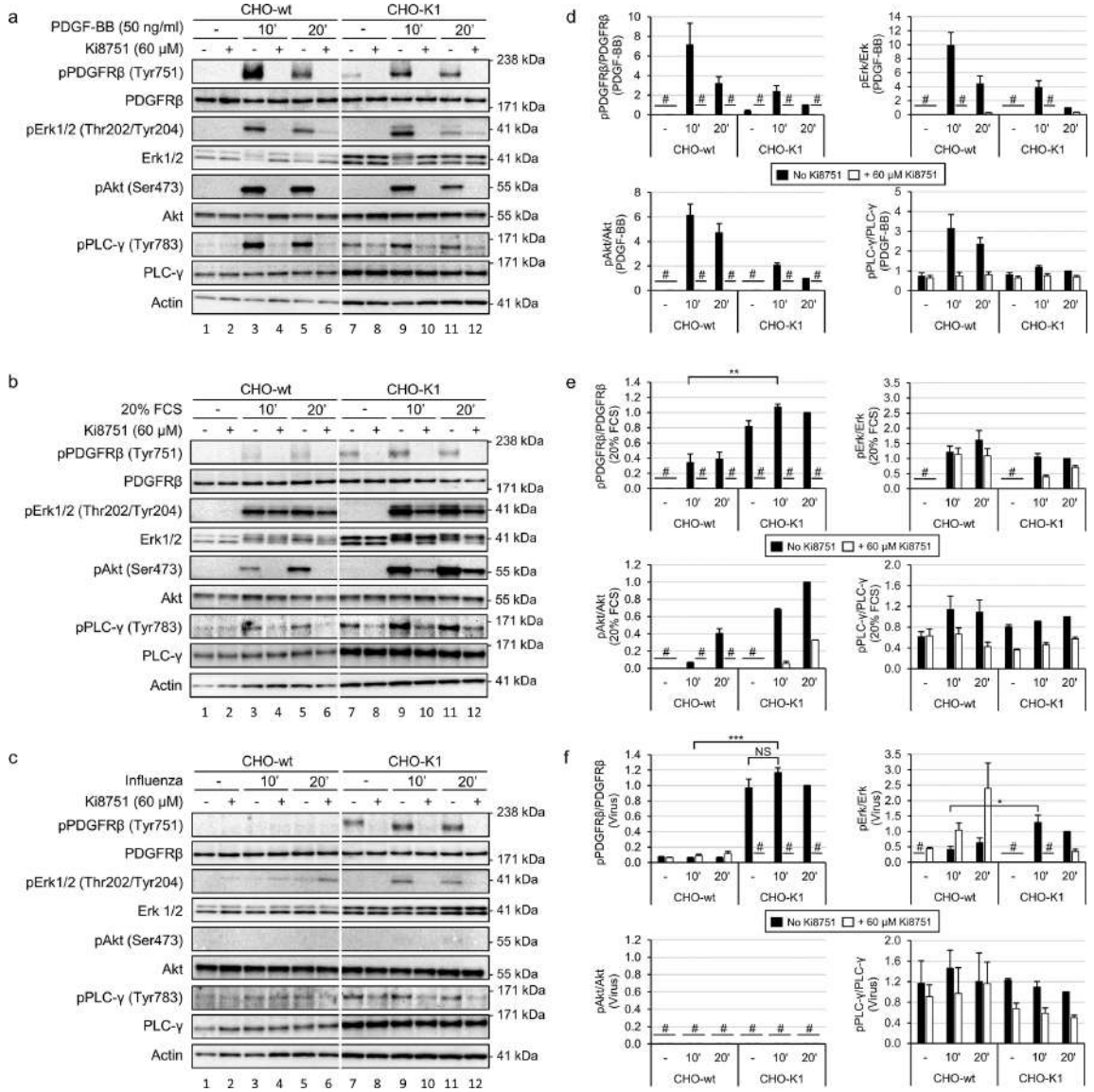

Fig. 8. PDGFRβ activation pathway in CHO-wt and CHO-K1 cells. (a, b, c) After 60 min of serum starvation, the CHO cells were incubated for 15 min without compound (indicated with a dash) or with 60 µM Ki8751. The cells were processed for protein extraction immediately before adding a stimulant (condition: -) or after 10 or 20 min incubation with 50 ng PDGF-BB ml^{-1} (a), medium with 20 % FCS (b) or A/PR/8/34 influenza virus (c). The images shown are from one out of three experiments giving similar results. (d, e, f) Bar diagrams of the band intensities of the phosphoprotein divided by that for the matching total protein (band intensities were quantified relative to the CHO-K1 band at 20 min, not treated with Ki8751). *P<0.05, **P<0.01, ***P<0.005 (two-sided Student's t-test). Data are the mean±SEM (N=3).

We also analysed the impact of influenza virus infection on three downstream pathways, i.e. Raf/MEK/Erk, PI3K/Akt and PLC-γ. In CHO-K1 cells, entering virus induced manifest Erk1/2 activation that was fully prevented by Ki8751 (Fig. 8c: lanes 10 and 12). In infected CHO-wt cells, Erk1/2 activation was significantly lower and, intriguingly, enhanced by Ki8751 (Fig. 8c: lane 6). This is reminiscent of reports [60, 61] that imatinib induces Erk1/2 phosphorylation in cell types showing low PDGFRβ activation. A similar phenomenon may occur here in influenza virus-infected CHO-wt cells. With the strong PDGF-BB stimulus, these cells did show inhibition of Ki8751 on phosphorylation of PDGFRβ and downstream effectors. This raises an apparent discrepancy, because in CHO-wt cells the inhibitory effect of Ki8751 on virus entry (Fig. 4c) seems not to be explained by inhibition of PDGFRβ phosphorylation. Perhaps Ki8751 may also affect the conformation or function of PDGFRβ in a way beyond blocking its phosphotransferase activity, as

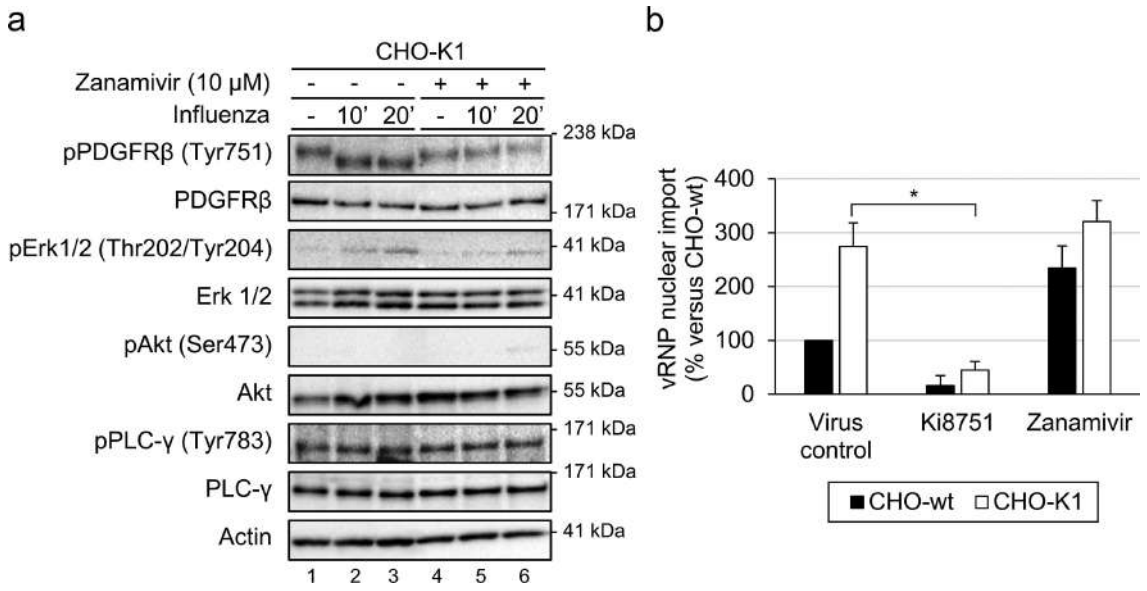

Fig. 9. Influenza virus NA desialylates phospho-PDGFRβ. (a) Receptor desialylation is inhibited by zanamivir. After 60 min of serum starvation, CHO-K1 cells were incubated for 15 min with 10 μM zanamivir (+) or without compound (-). The cells were processed for protein extraction before adding the virus (condition: '-'), or after 10 or 20 min of incubation with virus, during which zanamivir remained present. During incubation with zanamivir and virus, serum-free medium was maintained to ensure starving conditions. (b) The inhibitory effect of zanamivir on influenza virus entry in CHO-wt and CHO-K1 cells, estimated by vRNP nuclear import after 1 h of incubation at 35 °C. Quantitative confocal microscopy was carried out after dual nuclear staining for viral NP and DAPI. In three separate experiments, three images (each containing ~120 cells) were taken from each condition to quantify the green fluorescent signal in the nucleus.

described for other protein kinase inhibitors [62]. Finally, influenza virus did not provoke PI3K/Akt activation in CHO-wt or CHO-K1 cells, despite the fact that this pathway was clearly activated by PDGF-BB or 20 % FCS. The virus also did not affect PLC-γ.

To summarize, this analysis revealed that virus infection of CHO-K1 cells enhanced phosphorylation of PDGFRβ combined with strong activation of the Raf/MEK/Erk pathway. These effects were significantly lower in CHO-wt cells. In CHO-K1 cells, Ki8751 potently inhibited phosphorylation of PDGFRβ and its downstream effectors. This consolidates our conclusion that Ki8751 exerts its anti-influenza virus activity via inhibition of the PDGFRβ receptor.

Upon entry, the viral NA desialylates the phosphorylated PDGFRβ receptor

In Western blot experiments, virus infection of CHO-K1 cells proved to be associated with a clear downward shift in the band of phospho-PDGFRβ (Fig. 9a: lanes 2 and 3 in the top image). We presumed desialylation of PDGFRβ by the NA of cell-bound influenza virus particles, analogous to a study in which *Clostridium* NA was found to desialylate PDGFRβ, resulting in a ±5 kDa size reduction [63]. This hypothesis was verified with zanamivir. The band of phospho-PDGFRβ was located at exactly the same size in zanamivir-treated infected cells (Fig. 9a: lanes 5 and 6) compared to the uninfected condition (Fig. 9a: lane 1). This proves that the viral NA desialylates the PDGFRβ receptor when the virus binds at membrane domains in which PDGFRβ is in an activated state. It also implicates close proximity of virus and PDGFRβ during virus uptake.

Next, we analysed the effect of zanamivir on virus entry, using nuclear NP staining at 1 h p.i. Ki8751 was included for comparison. Zanamivir produced a slight increase in virus entry in CHO-wt but not in CHO-K1 cells (Fig. 9b). Upon virus binding, NA plausibly desialylates many different glycoproteins besides PDGFRβ. However, this result indicates that virus entry in CHO-wt cells is more affected by NA desialylation compared to that in CHO-K1 cells.

Influenza virus follows diverse internalization pathways in CHO-wt and CHO-K1 cells

Different endocytosis inhibitors were used to investigate whether the virus entry route(s) might differ in CHO-wt and CHO-K1 cells. Our data confirmed that dynamin-dependent virus uptake (sensitive to dynasore [12]) and macropinocytosis (sensitive to the Na^+/H^+ exchange blocker EIPA) can function in parallel (Fig. S5a). However, because both inhibitors are known to affect also other uptake pathways [64, 65], these results should be interpreted with care. The stronger effect of EIPA in 10 % FCS compared to 0.4 % FCS agrees with the report that macropinocytosis is stimulated by serum [16]. Virus entry was also reduced by three other molecules (Fig. S5b): chlorpromazine, an inhibitor of

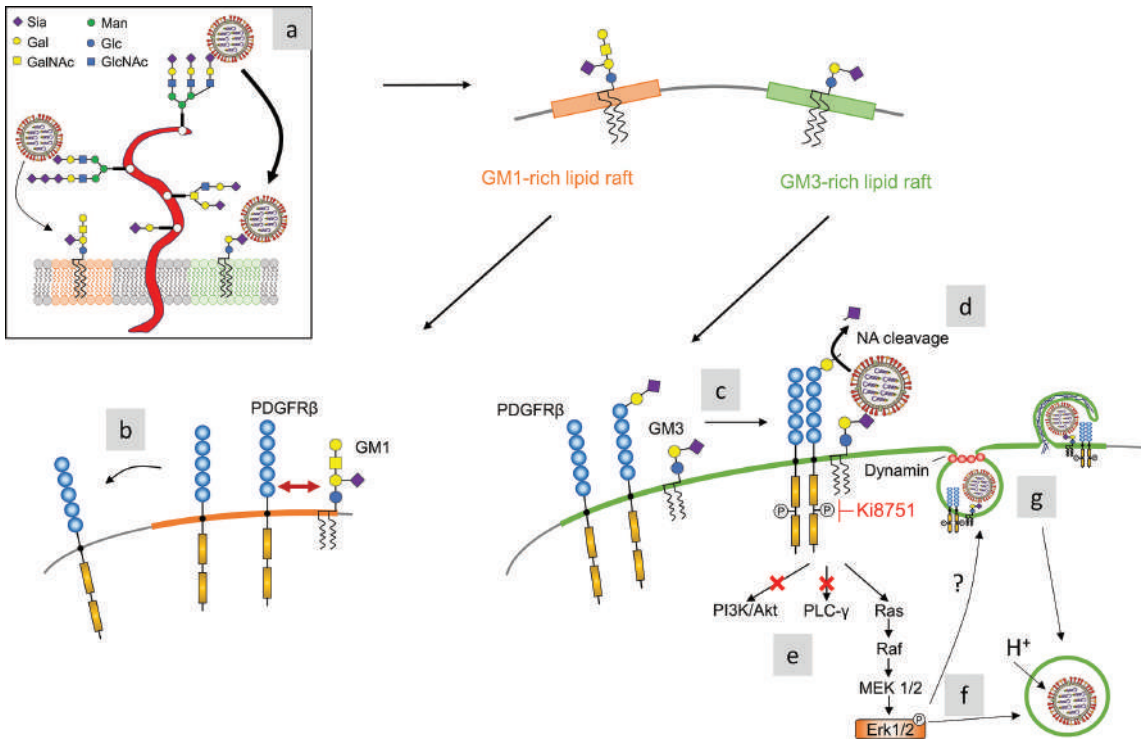

Fig. 10. Proposed model summarizing our findings in connection to other reports. (a) After the viral HA first anchors to membrane-distal sialic acid termini of cell surface glycans, influenza virus may be drawn towards membrane-proximal GM1 and GM3 gangliosides [55] which are located in different lipid rafts [68, 70]. Due to the unsubstituted sialylated headgroup in GM3, the virus probably prefers $GM3^+$ rafts. (b) By expelling PDGFRβ out of the lipid rafts, GM1 prevents dimerization and autophosphorylation of this receptor [56]. (c) In contrast, GM3 stimulates PDGFRβ activation [23, 57], explaining more efficient internalization of the virus at $GM3^+$ rafts. (d) Upon virus binding, the viral NA desialylates the phosphorylated PDGFRβ receptor, which might possibly trigger endocytosis. (e) Phosphorylation of PDGFRβ (which is effectively inhibited by Ki8751) leads to activation of the Raf/MEK/Erk cascade. We did not see activation of the PI3K/Akt or PLC-γ pathways in contrast to other reports [74, 75]. (f) Phosphorylated Erk1/2 may stimulate dynamin-dependent virus uptake and/or an intra-endosomal event required by the virus, such as V-ATPase-dependent endosome acidification [75]. (g) In our CHO cell assays, dynamin-dependent internalization and macropinocytosis appeared to function in parallel.

clathrin-mediated endocytosis [15]; nocodazole, a microtubule disrupting agent that interferes with endosome trafficking [66]; and rhosin, an inhibitor of RhoA GTPase [67]. Finally, cholesterol depletion with methyl-β-cyclodextrin prior to virus infection was performed to investigate the importance of lipid rafts. The reduction by methyl-β-cyclodextrin was more pronounced in CHO-K1 compared to CHO-wt cells (Fig. S5c), which aligns with our finding that the PDGFRβ/GM3 route for virus entry is more active in CHO-K1 cells.

In combination, these inhibitor studies (which are limited by the promiscuous activity of some inhibitors used) did not point to any specific route as being predominant in either CHO-wt or CHO-K1 cells.

DISCUSSION

This study was initiated after identification of the PDGFRβ inhibitor Ki8751 in an influenza virus screen of 276 protein kinase inhibitors. For comparison, of 24 EGFR inhibitors, gefitinib was the only one found to be active. A similar screen to ours yielded the PDGFR inhibitor tyrphostin A9 [48], yet these authors did not investigate the signalling pathway. The >350-fold reduction in virus yield achieved by Ki8751 is >100-fold better than that reported for the broad RTK inhibitor genistein [18]. Hence, the strong effect of Ki8751 points to the PDGFRβ pathway as a suitable direction for host-targeting influenza therapy.

As to the role of PDGFRβ in virus replication, we found that the entering virus activates PDGFRβ in connection with two other players: membrane gangliosides and the viral NA. Virus entry proved significantly higher in GM3-rich CHO-K1 cells compared to GM1-rich CHO-wt cells. This virus preference correlates with the positive effect of GM3 on PDGFRβ signalling and opposite effect of GM1. GM3 and GM1 are located in separate raft compartments of the cell membrane [68–70] and have divergent RTK-regulating abilities [23]. GM1 causes receptor dispersion from GEM towards non-GEM domains [56]. Exogenous GM1 but not

GM3 inhibits dimerization (in other words, autoactivation) of PDGFRβ [57]. The positive effect of GM3 is supported by the observation that an anti-GM3 antibody inhibited PDGFRβ function [71]. Unlike GM1, GM3 possesses an unsubstituted sialylated headgroup. We therefore propose that the α-[2,3]-linked sialic acid moiety of GM3 may be accessible to the viral HA to promote virus binding at GM3-positive lipid rafts, as evidenced by co-localization of virus and GM3 in the cell membrane of CHO-K1 cells. The finding that CHO-K1 cells show more efficient uptake of influenza pseudoparticles consolidates our interpretation that the viral HA and NA are responsible for this GM3-stimulated entry. A previous investigation [18] indicated that HA-mediated virus binding induces lipid raft clustering, resulting in RTK activation and a signalling cascade that enables virus internalization. It was proposed that the virus may use different RTKs depending on which RTK types are present on the cells under study. Here we demonstrate that the RTK–ganglioside interplay is an additional contributor to cell line-dependent virus uptake. Taking this evidence together, we hypothesize that the HA-mediated interaction with cell glycans may occur at two consecutive levels (see proposed model in Fig. 10), the first being anchorage to sialylated glycoproteins that protrude from the cell membrane, and the second being contact with GM3-rich lipid rafts where appropriate RTKs like PDGFRβ are present.

We are the first to describe an association between the viral NA and RTK-mediated entry, in which NA desialylates the activated PDGFRβ receptor. Our finding implicates close contact between the virus and RTK receptor. The fact that all phospho-PDGFRβ protein was desialylated is a strong indication that virus binding, desialylation and PDGFRβ activation are coupled. The complex and ambiguous role of NA in virus internalization was reported previously, yet the underlying mechanism was not revealed [72].

Regarding the downstream pathways, we found that PDGFRβ/GM3-controlled virus entry leads to strong and early activation of Erk1/2; no effect was seen on the PI3K/Akt and PLC-γ pathways. Erk1/2 activation was much stronger in CHO-K1 compared to CHO-wt cells, concurring with the report that PDGF-induced Erk activation is disturbed in GM1-expressing cells [56]. Pleschka *et al.* [73] reported biphasic Raf/MEK/Erk activation in influenza virus-infected MDCK cells, with peaks at 5–30 min and 8–10 h p.i. The late Erk activation was linked to nuclear export of influenza vRNPs. In A549 cells (which are rich in GM1 but scarce in GM3), influenza virus was shown to induce early PLC-γ1 [74] or PI3K/Akt activation [75]. This suggests that PDGFRβ-dependent virus uptake into CHO or MDCK cells involves the Raf/MEK/Erk pathway, whereas in A549 cells the RTK route is linked to PI3K/Akt or PLC-γ. This could be related to the specific route that is taken by the RTK receptor for its internalization [76] and is being hijacked by influenza virus. We currently have no insight into which endocytic pathway is followed when the virus enters via PDGFRβ/GM3. In our CHO cells, virus appears to enter via both dynamin-dependent pathways and macropinocytosis; the latter was reported as more sensitive to RTK inhibitors [16]. Intriguingly, in airway smooth muscle cells, PDGFRβ and downstream Erk signalling appears to be controlled by caveolae-dependent endocytosis [77]; contradictory reports exist on the involvement of this lipid raft-mediated route in influenza virus uptake [14, 15].

The different virus entry efficiency in CHO-K1 and CHO-wt cells could explain some enigmatic findings in the literature. In a follow-up study [72] on the poorly understood requirement of *N*-glycans for influenza virus entry [78], striking differences were seen between two glycosylation-defective CHO mutants. This might be related to their GM1/GM3 levels and PDGFRβ activation capacity. PDGFRβ is heavily *N*-glycosylated [79]. In CHO-wt cells, interactions between these *N*-glycans and GM3 (such as described for EGFR [80, 81]) may be crucial to strengthen the binding of PDGFRβ to the scarcely expressed GM3 ganglioside. The interaction may be stronger for sialylated PDGFRβ, as suggested by our observation that in CHO-wt cells virus entry is slightly increased when zanamivir prevents desialylation by NA. Viewed from a broader angle, our study underlines the importance of knowing the precise passage history when using CHO cells in influenza virus research.

We infer that the PDGFRβ/GM3 route for influenza virus uptake may also occur *in vivo*, as both PDGFRβ and GM3 are expressed in human lung tissue [82–84]. Our initial objective was to identify protein kinase inhibitors with relevance for antiviral drug development. Among the few active molecules identified, Ki8751 stood out as an attractive hit with quite selective and broad activity against influenza A and B virus. PDGFRβ inhibitors are under consideration for the treatment of asthma [85, 86]; clinical safety may be improved by developing drugs for inhalation [87]. Secondary evaluation of such PDGFRβ blockers for their potential effect on influenza virus replication seems warranted.

To conclude, recognition of influenza virus inhibition by the PDGFRβ inhibitor Ki8751 led us to reveal an as yet unknown aspect of influenza virus internalization, namely the interplay between viral HA and NA, and PDGFRβ in combination with GM3 ganglioside. Our findings shed new light on the multifactorial virus entry pathway, besides providing a new direction for host-targeting influenza therapeutics.

Funding information
P. V. acknowledges a PhD fellowship (teaching assistant) from KU Leuven – University of Leuven. E. V. holds a research grant from the Flemish Fonds voor Wetenschappelijk Onderzoek (FWO grant no. 1509715 N).

Acknowledgements
The authors wish to thank Wim van Dam for excellent technical assistance, and Geert Schoofs and Tati De Araujo Nogueira for guidance on some FACS and Western blot procedures. We thank R. Webster, G. Maertens and D. Daelemans for providing plasmid materials.

Conflicts of interest

The authors declare that there are no conflicts of interest.

References

1. World Health Organization. Influenza (seasonal) - Fact sheet No. 211. 2018. Available from: http://www.who.int/mediacentre/factsheets/fs211/en/.
2. Treanor JJ. Clinical practice. Influenza vaccination. *N Engl J Med* 2016;375:1261–1268.
3. Nguyen-van-Tam JS, Venkatesan S, Muthuri SG, Myles PR. Neuraminidase inhibitors: who, when, where? *Clin Microbiol Infect* 2015; 21:222–225.
4. Moscona A. Global transmission of oseltamivir-resistant influenza. *N Engl J Med* 2009;360:953–956.
5. Naesens L, Stevaert A, Vanderlinden E. Antiviral therapies on the horizon for influenza. *Curr Opin Pharmacol* 2016;30:106–115.
6. World Health Organization. Research needs for the Battle against Respiratory Viruses (BRaVe) - meeting report 2012. 2012. Available from: http://www.who.int/influenza/patient_care/clinical/BRaVE_meeting_report_november2012.pdf.
7. Tripathi S, Pohl MO, Zhou Y, Rodriguez-Frandsen A, Wang G *et al.* Meta- and orthogonal integration of influenza "omics" data defines a role for UBR4 in virus budding. *Cell Host Microbe* 2015;18:723–735.
8. Vanderlinden E, Naesens L. Emerging antiviral strategies to interfere with influenza virus entry. *Med Res Rev* 2014;34:301–339.
9. Fujioka Y, Nishide S, Ose T, Suzuki T, Kato I *et al.* A sialylated voltage-dependent Ca^{2+} channel binds hemagglutinin and mediates influenza A virus entry into mammalian cells. *Cell Host Microbe* 2018;23:809–818.
10. Edinger TO, Pohl MO, Stertz S. Entry of influenza A virus: host factors and antiviral targets. *J Gen Virol* 2014;95:263–277.
11. Byrd-Leotis L, Cummings RD, Steinhauer DA. The interplay between the host receptor and influenza virus hemagglutinin and neuraminidase. *Int J Mol Sci* 2017;18:1541.
12. Mercer J, Schelhaas M, Helenius A. Virus entry by endocytosis. *Annu Rev Biochem* 2010;79:803–833.
13. Zhang Y, Whittaker GR. Influenza entry pathways in polarized MDCK cells. *Biochem Biophys Res Commun* 2014;450:234–239.
14. Nunes-Correia I, Eulálio A, Nir S, Pedroso de Lima MC. Caveolae as an additional route for influenza virus endocytosis in MDCK cells. *Cell Mol Biol Lett* 2004;9:47–60.
15. Sieczkarski SB, Whittaker GR. Influenza virus can enter and infect cells in the absence of clathrin-mediated endocytosis. *J Virol* 2002;76:10455–10464.
16. de Vries E, Tscherne DM, Wienholts MJ, Cobos-Jiménez V, Scholte F *et al.* Dissection of the influenza A virus endocytic routes reveals macropinocytosis as an alternative entry pathway. *PLoS Pathog* 2011;7:e1001329.
17. König R, Stertz S, Zhou Y, Inoue A, Hoffmann HH *et al.* Human host factors required for influenza virus replication. *Nature* 2010; 463:813–817.
18. Eierhoff T, Hrincius ER, Rescher U, Ludwig S, Ehrhardt C. The epidermal growth factor receptor (EGFR) promotes uptake of influenza A viruses (IAV) into host cells. *PLoS Pathog* 2010;6: e1001099.
19. Casaletto JB, McClatchey AI. Spatial regulation of receptor tyrosine kinases in development and cancer. *Nat Rev Cancer* 2012;12: 387–400.
20. Lee IT, Yang CM. Inflammatory signalings involved in airway and pulmonary diseases. *Mediators Inflamm* 2013;2013:1–12.
21. Cahill KN, Katz HR, Cui J, Lai J, Kazani S *et al.* KIT inhibition by imatinib in patients with severe refractory asthma. *N Engl J Med* 2017;376:1911–1920.
22. Miljan EA, Bremer EG. Regulation of growth factor receptors by gangliosides. *Sci STKE* 2002;2002:re15.
23. Julien S, Bobowski M, Steenackers A, Le Bourhis X, Delannoy P. How do gangliosides regulate RTKs signaling? *Cells* 2013;2:751–767.
24. Matrosovich M, Suzuki T, Hirabayashi Y, Garten W, Webster RG *et al.* Gangliosides are not essential for influenza virus infection. *Glycoconj J* 2006;23:107–113.
25. Desbat B, Lancelot E, Krell T, Nicolaï MC, Vogel F *et al.* Effect of the β-propiolactone treatment on the adsorption and fusion of influenza A/Brisbane/59/2007 and A/New Caledonia/20/1999 virus H1N1 on a dimyristoylphosphatidylcholine/ganglioside GM3 mixed phospholipids monolayer at the air-water interface. *Langmuir* 2011;27:13675–13683.
26. Suzuki Y, Matsunaga M, Nagao Y, Taki T, Hirabayashi Y *et al.* Ganglioside GM1b as an influenza virus receptor. *Vaccine* 1985;3:201–203.
27. Suzuki Y. Gangliosides as influenza virus receptors. Variation of influenza viruses and their recognition of the receptor sialo-sugar chains. *Prog Lipid Res* 1994;33:429–457.
28. Kubo K, Shimizu T, Ohyama S, Murooka H, Iwai A *et al.* Novel potent orally active selective VEGFR-2 tyrosine kinase inhibitors: synthesis, structure-activity relationships, and antitumor activities of N-phenyl-N'-{4-(4-quinolyloxy)phenyl}ureas. *J Med Chem* 2005; 48:1359–1366.
29. Kimura K, Mori S, Tomita K, Ohno K, Takahashi K *et al.* Antiviral activity of NMSO3 against respiratory syncytial virus infection in vitro and in vivo. *Antiviral Res* 2000;47:41–51.
30. Matrosovich M, Matrosovich T, Carr J, Roberts NA, Klenk HD. Overexpression of the alpha-2,6-sialyltransferase in MDCK cells increases influenza virus sensitivity to neuraminidase inhibitors. *J Virol* 2003;77:8418–8425.
31. Ronca R, Giacomini A, di Salle E, Coltrini D, Pagano K *et al.* Long-pentraxin 3 derivative as a small-molecule FGF trap for cancer therapy. *Cancer Cell* 2015;28:225–239.
32. Stevaert A, Dallocchio R, Dessì A, Pala N, Rogolino D *et al.* Mutational analysis of the binding pockets of the diketo acid inhibitor L-742,001 in the influenza virus PA endonuclease. *J Virol* 2013;87: 10524–10538.
33. Hoffmann E, Neumann G, Kawaoka Y, Hobom G, Webster RG. A DNA transfection system for generation of influenza A virus from eight plasmids. *Proc Natl Acad Sci USA* 2000;97:6108–6113.
34. Vanderlinden E, Vanstreels E, Boons E, Ter Veer W, Huckriede A *et al.* Intracytoplasmic trapping of influenza virus by a lipophilic derivative of aglycoristocetin. *J Virol* 2012;86:9416–9431.
35. Naesens L, Vanderlinden E, Roth E, Jeko J, Andrei G *et al.* Anti-influenza virus activity and structure-activity relationship of aglycoristocetin derivatives with cyclobutenedione carrying hydrophobic chains. *Antiviral Res* 2009;82:89–94.
36. Stevaert A, Nurra S, Pala N, Carcelli M, Rogolino D *et al.* An integrated biological approach to guide the development of metal-chelating inhibitors of influenza virus PA endonuclease. *Mol Pharmacol* 2015;87:323–337.
37. Vanderlinden E, Göktas F, Cesur Z, Froeyen M, Reed ML *et al.* Novel inhibitors of influenza virus fusion: structure-activity relationship and interaction with the viral hemagglutinin. *J Virol* 2010; 84:4277–4288.
38. Reed LJ, Muench H. A simple method of estimating fifty per cent endpoints. *Am J Epidemiol* 1938;27:493–497.
39. Kamentsky L, Jones TR, Fraser A, Bray MA, Logan DJ *et al.* Improved structure, function and compatibility for CellProfiler: modular high-throughput image analysis software. *Bioinformatics* 2011;27:1179–1180.
40. Matsuda T, Cepko CL. Electroporation and RNA interference in the rodent retina in vivo and in vitro. *Proc Natl Acad Sci USA* 2004;101: 16–22.
41. Ulm JW, Perron M, Sodroski J, C Mulligan R. Complex determinants within the Moloney murine leukemia virus capsid modulate susceptibility of the virus to Fv1 and Ref1-mediated restriction. *Virology* 2007;363:245–255.

42. Jordan M, Schallhorn A, Wurm FM. Transfecting mammalian cells: optimization of critical parameters affecting calcium-phosphate precipitate formation. *Nucleic Acids Res* 1996;24: 596–601.
43. de Winter JCF. Using the Student's t-test with extremely small sample sizes. *Pract Assess, Res Eval* 2013;18:1–12.
44. Denisova OV, Söderholm S, Virtanen S, von Schantz C, Bychkov D *et al.* Akt inhibitor MK2206 prevents influenza pH1N1 virus infection in vitro. *Antimicrob Agents Chemother* 2014;58:3689–3696.
45. Hale BG, Knebel A, Botting CH, Galloway CS, Precious BL *et al.* CDK/ERK-mediated phosphorylation of the human influenza A virus NS1 protein at threonine-215. *Virology* 2009;383:6–11.
46. Söderholm S, Kainov DE, Öhman T, Denisova OV, Schepens B *et al.* Phosphoproteomics to characterize host response during influenza A virus infection of human macrophages. *Mol Cell Proteomics* 2016;15:3203–3219.
47. Droebner K, Pleschka S, Ludwig S, Planz O. Antiviral activity of the MEK-inhibitor U0126 against pandemic H1N1v and highly pathogenic avian influenza virus in vitro and in vivo. *Antiviral Res* 2011;92:195–203.
48. Kumar N, Liang Y, Parslow TG, Liang Y. Receptor tyrosine kinase inhibitors block multiple steps of influenza A virus replication. *J Virol* 2011;85:2818–2827.
49. Pohl MO, von Recum-Knepper J, Rodriguez-Frandsen A, Lanz C, Yángüez E *et al.* Identification of Polo-like kinases as potential novel drug targets for influenza A virus. *Sci Rep* 2017;7:8629.
50. Smallwood HS, Duan S, Morfouace M, Rezinciuc S, Shulkin BL *et al.* Targeting metabolic reprogramming by influenza infection for therapeutic intervention. *Cell Rep* 2017;19:1640–1653.
51. Holzberg M, Boergeling Y, Schräder T, Ludwig S, Ehrhardt C. Vemurafenib limits influenza A virus propagation by targeting multiple signaling pathways. *Front Microbiol* 2017;8:2426.
52. Root CN, Wills EG, McNair LL, Whittaker GR. Entry of influenza viruses into cells is inhibited by a highly specific protein kinase C inhibitor. *J Gen Virol* 2000;81:2697–2705.
53. Harcourt JL, Haynes LM. Establishing a liquid-covered culture of polarized human airway epithelial Calu-3 cells to study host cell response to respiratory pathogens in vitro. *J Vis Exp* 2013.
54. Rosales Fritz VM, Daniotti JL, Maccioni HJ. Chinese hamster ovary cells lacking GM1 and GD1a synthesize gangliosides upon transfection with human GM2 synthase. *Biochim Biophys Acta* 1997;1354:153–158.
55. Schnaar RL, Gerardy-Schahn R, Hildebrandt H. Sialic acids in the brain: gangliosides and polysialic acid in nervous system development, stability, disease, and regeneration. *Physiol Rev* 2014;94: 461–518.
56. Mitsuda T, Furukawa K, Fukumoto S, Miyazaki H, Urano T *et al.* Overexpression of ganglioside GM1 results in the dispersion of platelet-derived growth factor receptor from glycolipid-enriched microdomains and in the suppression of cell growth signals. *J Biol Chem* 2002;277:11239–11246.
57. Yates AJ, Saqr HE, van Brocklyn J. Ganglioside modulation of the PDGF receptor. A model for ganglioside functions. *J Neurooncol* 1995;24:65–73.
58. de Donatis A, Comito G, Buricchi F, Vinci MC, Parenti A *et al.* Proliferation versus migration in platelet-derived growth factor signaling: the key role of endocytosis. *J Biol Chem* 2008;283: 19948–19956.
59. Mitsui H, Takuwa N, Maruyama T, Maekawa H, Hirayama M *et al.* The MEK1-ERK map kinase pathway and the PI3-kinase-Akt pathway independently mediate anti-apoptotic signals in HepG2 liver cancer cells. *Int J Cancer* 2001;92:55–62.
60. Dong Y, Jia L, Wang X, Tan X, Xu J *et al.* Selective inhibition of PDGFR by imatinib elicits the sustained activation of ERK and downstream receptor signaling in malignant glioma cells. *Int J Oncol* 2011;38:555–569.
61. Fred RG, Boddeti SK, Lundberg M, Welsh N. Imatinib mesylate stimulates low-density lipoprotein receptor-related protein 1-mediated ERK phosphorylation in insulin-producing cells. *Clin Sci* 2015;128:17–28.
62. Hari SB, Merritt EA, Maly DJ. Conformation-selective ATP-competitive inhibitors control regulatory interactions and noncatalytic functions of mitogen-activated protein kinases. *Chem Biol* 2014;21: 628–635.
63. Hinek A, Bodnaruk TD, Bunda S, Wang Y, Liu K. Neuraminidase-1, a subunit of the cell surface elastin receptor, desialylates and functionally inactivates adjacent receptors interacting with the mitogenic growth factors PDGF-BB and IGF-2. *Am J Pathol* 2008; 173:1042–1056.
64. Park RJ, Shen H, Liu L, Liu X, Ferguson SM *et al.* Dynamin triple knockout cells reveal off target effects of commonly used dynamin inhibitors. *J Cell Sci* 2013;126:5305–5312.
65. Koivusalo M, Welch C, Hayashi H, Scott CC, Kim M *et al.* Amiloride inhibits macropinocytosis by lowering submembranous pH and preventing Rac1 and Cdc42 signaling. *J Cell Biol* 2010;188:547–563.
66. Lakadamyali M, Rust MJ, Babcock HP, Zhuang X. Visualizing infection of individual influenza viruses. *Proc Natl Acad Sci USA* 2003;100:9280–9285.
67. Jastrzębski K, Zdżalik-Bielecka D, Mamińska A, Kalaidzidis Y, Hellberg C *et al.* Multiple routes of endocytic internalization of PDGFRβ contribute to PDGF-induced STAT3 signaling. *J Cell Sci* 2017;130:577–589.
68. Fujita A, Cheng J, Hirakawa M, Furukawa K, Kusunoki S *et al.* Gangliosides GM1 and GM3 in the living cell membrane form clusters susceptible to cholesterol depletion and chilling. *Mol Biol Cell* 2007;18:2112–2122.
69. Markwell MA, Fredman P, Svennerholm L. Receptor ganglioside content of three hosts for Sendai virus. MDBK, HeLa, and MDCK cells. *Biochim Biophys Acta* 1984;775:7–16.
70. Janich P, Corbeil D. GM1 and GM3 gangliosides highlight distinct lipid microdomains within the apical domain of epithelial cells. *FEBS Lett* 2007;581:1783–1787.
71. Golard A. Anti-GM3 antibodies activate calcium inflow and inhibit platelet-derived growth factor beta receptors (PDGFbetar) in T51B rat liver epithelial cells. *Glycobiology* 1998;8:1221–1225.
72. de Vries E, de Vries RP, Wienholts MJ, Floris CE, Jacobs MS *et al.* Influenza A virus entry into cells lacking sialylated N-glycans. *Proc Natl Acad Sci USA* 2012;109:7457–7462.
73. Pleschka S, Wolff T, Ehrhardt C, Hobom G, Planz O *et al.* Influenza virus propagation is impaired by inhibition of the Raf/MEK/ERK signalling cascade. *Nat Cell Biol* 2001;3:301–305.
74. Zhu L, Ly H, Liang Y. PLC-γ1 signaling plays a subtype-specific role in postbinding cell entry of influenza A virus. *J Virol* 2014;88: 417–424.
75. Marjuki H, Gornitzky A, Marathe BM, Ilyushina NA, Aldridge JR *et al.* Influenza A virus-induced early activation of ERK and PI3K mediates V-ATPase-dependent intracellular pH change required for fusion. *Cell Microbiol* 2011;13:587–601.
76. Sigismund S, Confalonieri S, Ciliberto A, Polo S, Scita G *et al.* Endocytosis and signaling: cell logistics shape the eukaryotic cell plan. *Physiol Rev* 2012;92:273–366.
77. Gosens R, Stelmack GL, Dueck G, McNeill KD, Yamasaki A *et al.* Role of caveolin-1 in p42/p44 MAP kinase activation and proliferation of human airway smooth muscle. *Am J Physiol Lung Cell Mol Physiol* 2006;291:L523–L534.
78. Chu VC, Whittaker GR. Influenza virus entry and infection require host cell N-linked glycoprotein. *Proc Natl Acad Sci USA* 2004;101: 18153–18158.
79. Chen PH, Chen X, He X. Platelet-derived growth factors and their receptors: structural and functional perspectives. *Biochim Biophys Acta* 2013;1834:2176–2186.

80. **Kawashima N, Yoon SJ, Itoh K, Nakayama K.** Tyrosine kinase activity of epidermal growth factor receptor is regulated by GM3 binding through carbohydrate to carbohydrate interactions. *J Biol Chem* 2009;284:6147–6155.
81. **Yoon SJ, Nakayama K, Hikita T, Handa K, Hakomori SI.** Epidermal growth factor receptor tyrosine kinase is modulated by GM3 interaction with N-linked GlcNAc termini of the receptor. *Proc Natl Acad Sci USA* 2006;103:18987–18991.
82. **Aubert JD, Hayashi S, Hards J, Bai TR, Paré PD *et al.*** Platelet-derived growth factor and its receptor in lungs from patients with asthma and chronic airflow obstruction. *Am J Physiol* 1994;266: L655–L663.
83. **Narasimhan R, Murray RK.** Neutral glycosphingolipids and gangliosides of human lung and lung tumours. *Biochem J* 1979;179: 199–211.
84. **Hanqing M, Avrova N, Månsson JE, Molin K, Svennerholm L.** Gangliosides and neutral glycosphingolipids of normal tissue and oat cell carcinoma of human lung. *Biochim Biophys Acta* 1986;878: 360–370.
85. **Lewis CC, Chu HW, Westcott JY, Tucker A, Langmack EL *et al.*** Airway fibroblasts exhibit a synthetic phenotype in severe asthma. *J Allergy Clin Immunol* 2005;115:534–540.
86. **Humbert M, de Blay F, Garcia G, Prud'homme A, Leroyer C *et al.*** Masitinib, a c-kit/PDGF receptor tyrosine kinase inhibitor, improves disease control in severe corticosteroid-dependent asthmatics. *Allergy* 2009;64:1194–1201.
87. **Shaw DE, Baig F, Bruce I, Chamoin S, Collingwood SP *et al.*** Optimization of platelet-derived growth factor receptor (PDGFR) inhibitors for duration of action, as an inhaled therapy for lung remodeling in pulmonary arterial hypertension. *J Med Chem* 2016; 59:7901–7914.